AFOSR 2359

CONTRACT NO. AF 49(638)-44

PROJECT NO. 9781

LAMINAR, TRANSITIONAL, AND TURBULENT HEAT TRANSFER TO A CONE-CYLINDER-FLARE BODY AT MACH 8.0

by

Victor Zakkay and Clifton J. Callahan

FEBRUARY 1962

POLYTECHNIC INSTITUTE OF BROOKLYN

DEPARTMENT
of
AEROSPACE ENGINEERING
and
APPLIED MECHANICS

PIBAL REPORT No. 737

AFOSR 2359

LAMINAR, TRANSITIONAL, AND TURBULENT HEAT TRANSFER TO A CONE-CYLINDER-FLARE BODY AT MACH 8.0

by

Victor Zakkay and Clifton J. Callahan

This research was supported by the
United States Air Force through the
Air Force Office of Scientific Research
of the Office of Aerospace Research,
under Contract No. AF 49(638)-445,
Project No. 9781.

Polytechnic Institute of Brooklyn

Department of

Aerospace Engineering and Applied Mechanics

February 1962

PIBAL Report No. 737

LAMINAR, TRANSITIONAL, AND TURBULENT HEAT TRANSFER TO A CONE-CYLINDER-FLARE BODY AT MACH 8.0[†]

by

Victor Zakkay[*] and Clifton J. Callahan[**]

Polytechnic Institute of Brooklyn

SUMMARY

An experimental investigation of the laminar, transitional, and turbulent heat transfer rates over a conical cylindrical flared body is presented. Regions of favorable, zero, and adverse pressure gradient on the body are investigated. The experimental results are compared with the theories available in the literature.

The model chosen for this investigation is a cone-cylinder-flare configuration consisting of a 20° semi-vertex conical nose portion smoothly blended by a shoulder radius into a long cylindrical body and terminated by a smooth large radius flare.

The model was tested at a free stream Mach number of 8 and a Reynolds number of 1.6×10^5 to 0.3×10^5 per inch based on free stream

---

[†] This research was supported by the United States Air Force through the Air Force Office of Scientific Research of the Office of Aerospace Research, under Contract No. AF 49(638)-445, Project No. 9781.

[*] Research Assistant Professor, Aerospace Engineering

[**] Graduate Student, presently employed at the Curtiss Wright Corp., Wood-Ridge, New Jersey.

conditions. Various stagnation-to-wall temperature ratios were obtained by cooling the model prior to the test with liquid nitrogen. The stagnation-to-wall temperature ratios ranged from 10 to 3.3.

The theoretical predictions gave good results for the heat transfer rates in the laminar region, and fair prediction in the transitional and turbulent regimes extending over the shoulder and forward portion of the cylindrical body. Over the aft portion of the cylinder and over the flare the predictions are only qualitatively correct, and underestimate the heating rate by a factor as high as 2. Conversely, the "flat plate reference enthalpy" method is found more closely to predict the heat rates over the aft portion of the body, but increasingly to overestimate the heating rates over the forward portion of the cylinder.

A modified equation for the heat transfer coefficient in the transitional and fully turbulent region based on the F.P.R.E. method is then presented. This method gives good agreement with the experimental results presented here.

From the results the following is concluded: Cooling the wall delayed transition. By expanding the flow rapidly between the cone and the cylinder, the transition Reynolds number is reached very rapidly. By making a smooth transition between the cylinder and the flare, no separation occurred at the cylindrical flare junction. The transitional and turbulent heat transfer in the presence of an adverse pressure gradient may be predicted with sufficient accuracy by the F.P.R.E. method.

TABLE OF CONTENTS

LIST OF ILLUSTRATIONS

LIST OF ILLUSTRATIONS (Contd)

LIST OF TABLES

LIST OF SYMBOLS

C	$\rho\mu/\rho_e\mu_e$, density viscosity product ratio
C_f	$2\tau_w/\rho_e u_e^2$, local wall-friction coefficient
C_p	coefficient of specific heat at constant pressure
f'	u/u_e, velocity profile
g	h/h_{se}, enthalpy profile
h	enthalpy
H_c	boundary layer form factor
k	coefficient of thermal conductivity
K	$(h_{aw}-h_w)/(h_{se}-h_w)$
M	Mach number
N_{Nu}	$q_w C_{p_{se}} R_o/k_{se}(h_{se}-h_w)$, Nusselt number
N'_{Nu}	$q_w C'_p S/k'(h_{aw}-h_w)$, local Nusselt number based on reference enthalpy state
N_R	$\rho_{se}\sqrt{h_{se}}\, R_o/\mu_{se}$, Reynolds number
N'_R	$\rho' u_e S/\mu'$, local Reynolds number based on reference enthalpy state
$\tilde{N}_R$	$N_R \varphi_{se}^{\frac{1}{2}}$
$N_{R\theta}$	$\rho_e u_e \theta/\mu_e$, local Reynolds number based on boundary layer momentum thickness
P	pressure
$\bar{P}$	P_e/P_{se}
q	heat transfer per unit area per time
$\bar{r}$	r_o/R_o

LIST OF SYMBOLS (Contd)

r_o	local radius of body
R	specific gas constant
R_o	reference length, taken equal to 1/12 foot
S	surface coordinate, measured from the cone vortex
$\overline{S}$	S/R_o
$\tilde{S}$	transformed coordinate along body surface
T	temperature
u	velocity component parallel to surface
$\overline{u}$	$u_e/\sqrt{h_{se}}$
v	velocity component normal to surface
y	coordinate normal to body surface
$\overline{\beta}_{c.r.}$	pressure gradient parameter = $\frac{2\tilde{S}}{M_e}\frac{dM_e}{d\tilde{S}} = \left(\frac{h_{se}}{h_e}\right)\frac{2\tilde{S}}{u_e}\frac{du_e}{d\tilde{S}}$
γ	ratio of specific heats
δ_c	cone semi-vertex angle
δ^*	boundary layer displacement thickness
η	nondimensional coordinate normal to body surface, a similarity variable
θ	physical momentum thickness
Θ	transformed momentum thickness
μ	dynamic viscosity
$\overline{\mu}$	μ_e/μ_{se}
ρ	mass density
$\overline{\rho}$	ρ_e/ρ_{se}

LIST OF SYMBOLS (Contd)

σ	$C_p\mu/k$, Prandtl number
τ	shear stress
φ_{se}	$P_{se}/\rho_{se}h_{se} \approx (\frac{\gamma-1}{\gamma})$
Ψ	stream function

Subscripts

aw	adiabatic wall
e	local value external to boundary layer
n	conditions behind normal shock wave
s	stagnation state
trans	transition point
w	wall conditions
∞	free stream ahead of body
c.r.	Cohen and Reshotko

SECTION I

INTRODUCTION

In recent years, with the progress of hypersonic flight, the ability reliably to predict aerodynamic heating rates has become increasingly important; and concomitant with the developments in rockets and ballistic missiles, considerable attention has been given to the study of the boundary layer and heat transfer rates over axially symmetric bodies in high speed flow.

Specifically, the aim of the present work is to evaluate the accuracy with which several of the more recent analytical methods predict boundary layer development and heat transfer rates in the transitional and turbulent region at high Mach numbers. Several of these evaluations have been made at a relatively low Mach number, and it is the purposes of this report to extend these evaluations to a high Mach number.

For the laminar flow region a method of similar flow based on the numerical solutions of references 1 and 2 is employed together with the similarity transformations of reference 3. For the transitional and fully turbulent regimes a modification of the momentum integral method of reference 4, as suggested in reference 5, is used together with the Reynolds analogy corrected empirically for nonunity Prandtl number. The flat plate reference enthalpy method has also been used by various investigators and has yielded good results in some cases.

After formulation of the methods, solutions are obtained for a particular cone-cylinder-flare geometry, and finally the predicted results are compared with experiments. However, although applied to a specific body, it is also felt that the results are of general interest in ascertaining the applicability of the methods. For example, in the present work a region of particular interest is the junction of the conical surface with the cylindrical body, where, because of the radius of curvature, the pressure gradient becomes large, and thereby provides a critical test of the laminar and transitional theory. In addition, the compressing flow over the flare portion provides for examination of heat transfer theories under the influence of adverse pressure gradients.

The effect of a cold wall is studied, and its effect on the transitional Reynolds number is also given.

Some experimental heat transfer results have been reported in reference 6, 7, and 8 from free flight tests. In this report the experimental results have been obtained in the PIBAL Mach 8 wind tunnel. The stagnation pressure ranged from 600 to 100 psia, and the stagnation temperature was approximately 2000°R. The Reynolds number based on free stream conditions ranged from 1.6×10^{6}/into to $.25 \times 10^{6}$/inch.

This work has been initiated by Dr. Antonio Ferri, and the authors wish to thank him for his suggestions and discussions in the work reported here. Grateful acknowledgment is due to Drs. Paul A. Libby and Robert J. Cresci for their stimulating discussion.

SECTION II

MODEL DESIGN AND TESTING PROCEDURE

The experimental program was conducted in the hypersonic facility of the Polytechnic Institute of Brooklyn Aerodynamics Laboratory. The tests were conducted at a Mach number of 8, in a range of stagnation pressures ranging between 100 and 600 psia, and at a stagnation temperature of approximately 2000°R. The stagnation to wall temperature of the model was varied from T_o/T_w from 3.2 to 10 by cooling the skin temperature of the model with liquid nitrogen prior to the test. The range of free stream Reynolds number per inch for the tests presented here is 1.6×10^5/in. x 0.25×10^5/in.

A schematic drawing of the model tested is shown in Fig. 1. The model consists of a pointed conical portion having a half angle of 20 degrees. This conical portion terminates at an $\bar{S}$ of 4.7 (where $\bar{S}$ is S/R_o and R_o is a reference length taken to be 1"). The conical portion is blended within a cylindrical portion by means of a segment of a circular arc. The equation representing the geometry of this circular arc in terms of $\bar{r}$ is given as

$$4.696 \leq \bar{S} \leq 6.616$$

$$\bar{r} = -3.563 + 5.5 \cos [68.92 - 10.42\bar{S}]$$

The circular arc terminates with the cylinder at $\bar{S}$=6.616. The cylindrical portion continues then to an $\bar{S}$ of 23.99. At this point the cylindrical body flares out from a diameter of 3.875" to a diameter of

5.95" in a distance of 12". Similarly in this case the flare is also expressed by a segment of a circle and is given in terms of $\bar{r}$ by the following equation:

$$23.99 \leqq \bar{S} \leqq 36.19$$

$$\bar{r} = 71.854 - 69.916 \cos[19.66 - 0.82\bar{S}] .$$

The model was constructed of 304 stainless steel having a wall thickness of 0.050". Table II presents the location of the thermocouples and the pressure taps. The pressure taps and thermocouples were located at two planes at a radial angle of 30°. A copper tube, having a one-half inch diameter and having several holes 1/32" in diameter, was placed at the center line of the model along all its length for the purpose of cooling the model with liquid nitrogen prior to the test.

The heat transfer to the model was determined by the transient technique. The model is initially at constant temperature; then the initial heat pulse was obtained by starting the flow suddenly. The derivative of the surface temperature with respect to time was measured at 0.2 seconds from starting and used in determining the heat transfer to the surface of the model. For this condition the temperature of the model was almost uniform, therefore lateral conduction could be neglected. In the case where a temperature less than the ambient temperature was desired prior to the test, the following procedure was followed. The tunnel was evacuated to a vacuum of 29 inches of mercury, and the copper tube within the model was connected

to a liquid nitrogen bottle. Cooling of the model continued until a uniform temperature on the model was reached. By maintaining a vacuum in the wind tunnel, no frosting occurred within or at the surface of the model.

The data are presented in terms of a Nusselt number, defined by

$$N_{Nu} = q_w(C_p)_{se} R_o / k_{se}(h_{se}-h_w)$$

and by a Reynolds number parameter

$$\tilde{N}_R = N_R \sqrt{P_s/\rho_{se}h_{se}} = N_R \varphi_{se}^{\frac{1}{2}}$$

$$N_R = \rho_{se}\sqrt{h_{se}}\, R_o/\mu_{se}$$

$$\varphi_{se} = P_{se}/\rho_{se}h_{se}$$

Four test conditions are presented in the report,

Run No.	P_{o_∞} (psia)	T_w °R
1	590	520
2	200	520
3	100	520
4	600	180

All the tests were performed at a stagnation temperature of approximately 1800°R.

SECTION III

PRESSURE DISTRIBUTION AND HEAT TRANSFER RESULTS

The pressure distribution results are presented in Fig. 2 in the form of P_e/P_{se} versus $\bar{S}$, where P_{se} is the stagnation pressure behind the conical shock. The Mach number on the conical portion is M_e=4.24, which agrees well with the Kopal value. A Mach number of 6.80 is reached after the expansion; this value is somewhat higher than the value obtained with a standard Prandtl-Meyer expansion. This is due to the overexpansion which occurs at the beginning of the cylinder. At the end of the flare the flow is compressed from a Mach number of 6.8 to a Mach number of 5.84. Included in the figure is the comparison of the pressure distributions on the flare with the tangent cone method (Table I).

The experimental heat transfer data are presented in three different forms in order to distinguish the effects of laminar, transitional, and turbulent heat transfer. The results are presented in terms of the Nusselt and Reynolds numbers due to their insensitivity with respect to enthalpy ratios.

It is well-known that for laminar flow N_{Nu} varies with $\tilde{N}_R^{\frac{1}{2}}$ while for turbulent flow the variation is $N_{Nu} \sim \tilde{N}_R^{4/5}$.

In order to indicate the laminar part of the variation the heat transfer data is presented in Figs. 3-5 in the forms of $N'_{Nu}/N_R'^{\frac{1}{2}}$ versus $\bar{S}$. Where

$$N'_{Nu} = \frac{q_w (C_p)' S}{(h_{aw}-h_w)K'} \qquad (1)$$

$$\tilde{N}'_{Re} = \frac{\rho' u_e S}{\mu'} \tag{2}$$

and

$$\bar{S} = \frac{S}{R_o} \qquad (R_o=1)$$

It is seen that by presenting the data in this form both the laminar part and transitional point on the body may easily be indicated. Figs. 6-9 present the variation of N'_{Nu} with N'_R for laminar transitional and turbulent heat transfer results for the full body length. For comparison with the various theories the experimental results are again presented in Figs. 10 and 11 for test no. 1 in the form of N_{Nu} and N'_{Nu} versus $\bar{S}$, where

$$N_{Nu} = \frac{q_w C_{p_{se}} R_o}{k_{se}(h_{se}-h_w)} \tag{3}$$

SECTION IV

THEORETICAL ANALYSIS

The more commonly employed method for computing the laminar boundary layer is to use the transformation of reference 3 for similar solutions, with the numerical solution of reference 1. The above method yields good results when the pressure gradient $\bar{\beta}$, as defined in the equation below, does not vary significantly along the body:

$$\overline{\beta}_{c.r.} = \frac{2\tilde{S}}{M_e}\frac{dM_e}{d\tilde{S}} = \left(\frac{h_{se}}{h_e}\right)\overline{\beta}_{Lees} \tag{4}$$

where

$$\overline{\beta}_{Lees} = \frac{2\tilde{S}}{u_e}\frac{du_e}{d\tilde{S}} \tag{5}$$

For larger values of $\overline{\beta}$ ($\overline{\beta} > 2$) the numerical solutions of reference 2 have to be used. The initial estimates of laminar heat transfer were based on the assumption that $\overline{\beta} = 0$.

In terms of the nondimensional quantities given in reference 5, the theoretical results for the laminar heat transfer of reference 3 give

$$\frac{N_{Nu}}{\tilde{N}_R^{\frac{1}{2}}} = \frac{\sqrt{2}}{2}\left(\frac{g_w'}{1-g_w}\right)\frac{\overline{\rho}\,\overline{\mu}\,\overline{u}\,\overline{r}}{\left[\int_0^{\overline{S}}\overline{\rho}\,\overline{\mu}\,\overline{u}\,\overline{r}^2 d\overline{S}\right]^{\frac{1}{2}}}\frac{\sigma^{\frac{2}{3}}}{\varphi_{se}^{\frac{1}{4}}} \tag{6}$$

for the case $\overline{\beta}=0$, the similar solutions of reference 1 give

$$\left(\frac{g_w'}{1-g_w}\right) = 0.470 \tag{7}$$

$$\frac{N_{Nu}}{\tilde{N}_R^{\frac{1}{2}}} = \frac{0.67}{2}\frac{\overline{\rho}\,\overline{\mu}\,\overline{u}\,\overline{r}}{\left[\int_0^{\overline{S}}\overline{\rho}\,\overline{\mu}\,\overline{u}\,\overline{r}^2 d\overline{S}\right]^{\frac{1}{2}}}\frac{\sigma^{\frac{2}{3}}}{\varphi_{se}^{\frac{1}{4}}} \tag{8}$$

Over the conical nose portion of the model this result reduced to the simple form

$$\frac{N_{Nu}}{\tilde{N}_R^{\frac{1}{2}}} = \frac{0.67}{2}\sqrt{3}\left(\frac{\bar{\rho}\,\bar{\mu}\,\bar{u}}{\bar{S}}\right)^{\frac{1}{2}} \frac{\sigma^{\frac{2}{3}}}{\varphi_{se}^{\frac{1}{4}}} \tag{9}$$

From these computations the predicted laminar heating ratio for the present body are presented in Fig. 10. The agreement between these results and the experiments are seen to be good.

The laminar heat transfer over the conical portion of the model may also be calculated in terms of the reference enthalpy.method. In terms of the notation presented in reference 5, the laminar heat transfer is

$$N'_{Nu} = 0.332\,(\sigma'^{\frac{1}{3}})(N'_{Re})^{\frac{1}{2}} \quad \text{(flat plate)} \tag{10}$$

$$N'_{Nu} = 0.576\,\sigma'^{\frac{1}{3}}(N'_{Re})^{\frac{1}{2}} \quad \text{(cone)} \tag{11}$$

(prime quantities indicate properties evaluated at the reference conditions).

The results of these analyses are presented in Figs. 2-9 for the tests reported here.

A. Laminar momentum thickness and the transition point

At the outset of this work, it was known from experimental observations that transition from laminar to turbulent flow occurred approximately at a local Reynolds number, based on momentum thickness, equal to approximately 600.[9] To establish the location of

the transition point for the theoretical analysis it became necessary then to calculate the development of the laminar momentum thickness over the body.

1. Solution by exact similarity

From the definition of the momentum defect thickness

$$\theta = \int_0^\infty \frac{\rho u}{\rho_e u_e} \left(1 - \frac{u}{u_e}\right) dy \tag{12}$$

and the local Reynolds number

$$N_{R\theta} = \frac{\rho_e u_e}{\mu_e} \theta \tag{13}$$

the transformation of Lees results in

$$\theta = \frac{(2\tilde{S})^{\frac{1}{2}}}{\rho_e u_e r_o} \Theta \tag{14}$$

and

$$N_{R\theta} = \frac{(2\tilde{S})^{\frac{1}{2}}}{\mu_e r_o} \Theta \tag{15}$$

where Θ is the transformed momentum thickness

$$\Theta = \int_0^\infty f'(1-f')d\eta \tag{16}$$

Employing the method of similar flows, the value of Θ is computed from the solution of the velocity profile f', and hence Θ is functionally dependent on the similarity parameters $\overline{\beta}$ and g_w.

In the present work, for the 500°R wall and 1800°R stagnation temperatures upon which the analytical treatment is based, the enthalpy ratio gives

$$g_w = 0.2772,$$

and as computed from the similar solutions of references 1 and 2, Fig. 12 presents the corresponding values of Θ as a function of the pressure gradient similarity parameter $\overline{\beta}$.

Over the conical portion of the body, the relation between body radius and the surface coordinate is given explicitly by

$$r_o = S \sin \delta_c$$

Hence, the transformed surface coordinate $\tilde{S}$ becomes

$$\tilde{S} = \rho_e u_e \mu_e \frac{S^3}{3} \sin^2 \delta_c \tag{17}$$

and by Eqs. (14) and (15), the physical momentum thickness and local Reynolds number are given by

$$\theta = \left(\frac{2}{3} \frac{\mu_e}{\rho_e u_e} S\right)^{\frac{1}{2}} \Theta \tag{18}$$

and

$$N_{R\theta} = \left(\frac{2}{3} \frac{\rho_e u_e}{\mu_e} S\right)^{\frac{1}{2}} \Theta \tag{19}$$

where the transformed momentum thickness Θ is evaluated from Fig. 3 for $\overline{\beta} = 0$.

Over the shoulder region, however, the properties of the external flow are dependent on the assumed Prandtl-Meyer expansion. Further, a simple expression for r_o as a function of S is not easily written. Hence, in this region $\tilde{S}$, and thus θ and $N_{R\theta}$, had to be computed by numerical integration.

For this calculation, in keeping with the assumption of exact similarity, the value of $\overline{\beta}$ was supposed constant all along the body surface. Hence, while in fact the value of $\overline{\beta}$ varied locally, the transformed momentum thickness Θ was evaluted (as for the cone) at $\overline{\beta} = 0$.

The calculated distribution of $N_{R\theta}$ over the forward portion of the body, based on the presently prescribed external flow, is shown in Fig. 13a.

According to the transition criteria, $N_{R\theta} \approx 600$, Fig. 13a shows the predicted transition point to occur on the shoulder at S=6.07". This location on the body is illustrated in Fig. 1.

2. Solution by piecewise application of exact similarity

As mentioned in the above analysis, the flow expansion over the cone-cylinder shoulder region results in a large variation in the local value of the pressure gradient parameter $\overline{\beta}$. Since the previous analysis predicted the transition point to lie in this region, it became of interest to investigate the effect of $\overline{\beta}$ more rigorously.

The approach often employed to account for the effect of variations in $\overline{\beta}$ is the method of simple local similarity. However, in that method, since $\overline{\beta}$ depends only on the inviscid flow field, there is

no accounting for the previous history of boundary layer development.

To account in part for previous boundary layer history, it was decided to employ the method of piecewise exact similarity. This method insures continuity in the distribution of boundary layer momentum thickness, and is based upon an approach first suggested for incompressible flows by A.M.O. Smith.[10] The present development follows closely that of reference 2, except that in that case heat transfer was of primary concern, and the development was predicted on continuity in the distribution of the convection thickness.

The basic assumption underlying the present piecewise application of exact similarity is as follows:

> "An exact similar flow, not necessarily originating at the same point as the actual flow, may be applied within a finite interval of the body surface, and the effect of previous boundary layer history may be introduced by requiring continuity in the physical momentum thickness."

Specifically, let us consider a surface interval [1]-[2]. Within this interval the external velocity distribution is known from the potential flow field. Now, the physical momentum thickness and the external velocity at the start of the interval may be matched by a similar flow of arbitrary origin, and the arbitrariness of the origin may then be removed by requiring that the similar flow also satisfy the external velocity at the end of the interval. This similar flow may then be used

to predict the physical momentum thickness at the end of the interval.

Starting with a modified form of the transformation of Lees, for axisymmetric bodies

$$\eta = \frac{\rho_e u_e}{\sqrt{2(\tilde{S}-\tilde{S}_o)}} \int_o^y r_o \frac{\rho}{\rho_e} dy \tag{20}$$

and

$$\tilde{S} = \int_o^S \rho_e \mu_e u_e r_o^{\beta} dS , \tag{21}$$

where $\tilde{S}_o$ will be the effective origin of the similar flow.

The expression for $\overline{\beta}$ becomes in this case

$$\overline{\beta} = \frac{2(\tilde{S}-\tilde{S}_o)}{M_e} \frac{dM_e}{d\tilde{S}} ; \tag{22}$$

and hence, what has been said previously in connection with exact similar solutions, still applies.

Now, consistent with the assumption of exact similarity within a finite interval, $\overline{\beta}$ and $\tilde{S}_o$ are required to be constant. Hence, upon integrating Eq. (22) within an interval [1]-[2]

$$\frac{M_{e_2}}{M_{e_1}} = \left[1 + \frac{\tilde{S}_2 - \tilde{S}_1}{\tilde{S}_1 - \tilde{S}_o}\right]^{\frac{\overline{\beta}}{2}} \tag{23}$$

Also, employing the modified similarity transformation, the transformed momentum thickness Θ must also be constant within the interval, and thus for the end points of the interval

$$\theta_1 = \frac{\sqrt{2(\tilde{S}_1 - \tilde{S}_o)}}{(\rho_e u_e r_o)_1} \Theta , \tag{24}$$

and

$$\theta_2 = \frac{\sqrt{2(\tilde{S}_2 - \tilde{S}_o)}}{(\rho_e u_e r_o)_2} \Theta \tag{25}$$

Finally, upon manipulation of these relations, the working equations for the interval are obtained as

$$\frac{M_{e_2}}{M_{e_1}} = \left\{ 1 + 2(\tilde{S}_2 - \tilde{S}_1) \left[\frac{\Theta}{(\theta \rho_e u_e r_o)_1} \right]^2 \right\}^{\frac{\bar{\beta}}{2}} \tag{26}$$

and

$$\theta_2 = \frac{(\rho_e u_e r_o)_1}{(\rho_e u_e r_o)_2} \left(\frac{M_{e_2}}{M_{e_1}} \right)^{\bar{\beta}} \theta_1 \tag{27}$$

The first of these equations is solved by a trial-and-error procedure for $\bar{\beta}$, making use of the dependence of Θ on $\bar{\beta}$; and after obtaining $\bar{\beta}$, the physical momentum thickness, θ_2, at the end of the interval is found from the second equation.

For the present work, in the cone-cylinder shoulder region, application of this method of "Piecewise Exact Similarity" resulted in the schedule of similarity parameter $\bar{\beta}$ shown in Fig. 14. The corresponding distributions of the Reynolds number $N_{R\theta}$ has been superimposed on the plot of Fig. 13a.

From Fig. 13a, again employing the transition criteria

$N_{R\theta} \simeq 600$, the location of the transition point as predicted by the method of Piecewise Exact Similarity is found to occur at the station S=5.60 inches; for reference, this location has been indicated on the configuration drawing of Fig. 1.

Comparing the relative locations of the transition point as predicted by the method of exact similarity and the piecewise method of exact similarity respectively, the difference is seen to be small.

The slight difference in the predicted location of the transition point was considered to be well within the accuracy of the $N_{R\theta} \simeq 600$ transition criteria employed. Hence, it was concluded that the rigor of the method of piecewise solution was unnecessary, and from this stage on, the method of exact similarity was considered sufficiently accurate for all calculations associated with the laminar boundary layer.

The distribution of $N_{R\theta}$ in Fig. 13b has been calculated for test no. 1. In order to obtain the distribution of $N_{R\theta}$ over the body for the other test conditions the following equation is used:

$$\frac{N_{R\theta_2}}{N_{R\theta_1}} = \left(\frac{P_{s_{\infty_2}}}{P_{s_{\infty_1}}}\right)^{\frac{1}{2}} \tag{28}$$

By applying the above equation at each point of the body, the laminar distribution of $N_{R\theta}$ corresponding to any other free stream stagnation pressure p_{se_2} may be found.

The effect of free stream stagnation pressure on the transitional point for $N_{R\theta}$ =600 has been calculated from the above equation and is presented in Fig. 15.

From Figs. 13b and 15 it is seen that the transitional point persists for a larger range of stagnation pressures over the expansion section of the body than on the cylindrical section of the body.

It was of considerable interest to note that by expanding the flow rapidly around the cone $N_{R\theta}$ increases very rapidly, and reached a value of 600 at $\bar{S}$ equal to 5.6. On the other hand, if the cone extended further, the transitional point would occur at an $\bar{S}$ of 13.4 (this is consistent with the results presented in reference 9). These results are shown in Fig. 13b.

In the case of run 4, because of the cold wall conditions, transition occurs at an $N_{R\theta}$ of 1100. Cooling the wall thus has an effect on delaying transition, as has been observed by previous investigation.[10]

The following table gives a summary of the transitional point on the bodies for the tests reported here:

Test No.	$\bar{S}$	P_{o_∞}	T_{os}/T_w	$N_{R\theta}$
1	5.6	590	3.3	600
2	15	200	3.3	680
3	23	100	3.3	450
4	24	590	10	1100

B. The transitional and turbulent wall friction coefficient

To evaluate the wall friction coefficient in the transitional and fully turbulent flow regimes, the friction law modified in reference 5 was

adopted, i.e.:

$$\frac{C_f}{2} = \bar{\mu}\left[\frac{0.013}{N_{R\theta}^{\frac{1}{4}}} - \frac{B}{N_{R\theta}^{n}}\right] \tag{29}$$

This law is similar in form to that developed by Persh[4] through analogy with incompressible flow, but has been modified to include the law suggested by Vaglio-Laurin[12] for the fully developed turbulent flow of a compressible medium.

The constant B of this law is evaluated from the laminar flow, such that the friction coefficient $\frac{C_f}{2}$ remains continuous at the laminar to turbulent transition point, i.e.:

$$B = \left[N_{R\theta}^{n}\left(\frac{0.013}{N_{R\theta}^{\frac{1}{4}}} - \frac{C_f}{2}\frac{\mu_{se}}{\mu_e}\right)\right]_{trans.} \tag{30}$$

where

$$\left(\frac{C_f}{2}\right)_{trans.} = \frac{\mu_e r_o}{(2\tilde{S})^{\frac{1}{2}}} f''_w \tag{31}$$

and

$$[N_{R\theta}]_{trans} = \frac{(2\tilde{S})^{\frac{1}{2}}}{\mu_e r_o} \tag{32}$$

and therefore

$$\left[\frac{C_f}{2}\right]_{trans} = \frac{f''_w \Theta}{N_{R\theta}} \tag{33}$$

In the analysis of reference 5 the exponent n has been chosen to be 2.

Recently, reference 13 has indicated that the use of n=1 leads to better agreement for the transitional heat transfer in a favorable pressure gradient region. Therefore in the following analysis, in the favorable pressure gradient region, theoretical calculations were carried out for n=1 and 2 for one of the test conditions, and are presented in Table II. It is seen that, in this case, the variation of n on the transitional heat transfer has little effect. The reason for this is that the pressure gradient ($\bar{\beta}$) effect in this case is much more predominant than the effect of n. In the case of reference 13 the Mach number and pressure gradient were low in comparison to the results presented here.

C. The transitional and turbulent boundary layer

1. Modification of the method of Persh

For prediction of the transitional and turbulent boundary layer behavior, with inclusion of the effect of compressibility, body geometry, and pressure gradient, the present work employed a calculation scheme based on a modification of the method introduced by Persh.[4]

According to the method of Persh, a stepwise solution of the boundary layer momentum equation

$$\frac{d\theta}{dS} = \frac{C_f}{2} - \theta\left[\frac{\delta^*}{\theta}\frac{}{u_e}\frac{du_e}{dS} + 2\frac{1}{\rho_e}\frac{d\rho_e}{dS} + \frac{1}{r_o}\frac{dr_o}{dS}\right] \qquad (34)$$

is obtained through use of boundary layer form factors, which are based on a correlation of incompressible data.

In the present work, however, following the suggestion of

reference 5, the form factor was taken as*

$$H_c = \frac{\delta^*}{\theta} \approx 1$$

With this assumption then, the momentum equation reduced to the modified form

$$\frac{d\theta}{dS} = \frac{C_f}{2} - \theta\left[\frac{1}{u_e}\frac{du_e}{dS} + \frac{1}{\rho_e}\frac{d\rho_e}{dS} + \frac{1}{r_o}\frac{dr_o}{dS}\right]$$

$$= \frac{C_f}{2} - \theta\frac{d}{dS}\left[\ln\left(\frac{u_e}{\sqrt{h_{se}}}\frac{\rho_e}{\rho_{se}}\frac{r_o}{R_o}\right)\right] \qquad (35)$$

and combining this expression with the wall friction law, the local wall friction coefficient and the boundary layer development may be obtained by stepwise numerical solution.

An approximate method for solution is discussed in detail below. However, as stated in the general remarks, boundary layer solutions in the present work were obtained, together with heat transfer rate predictions, on the Bendix automatic computer. From these computations, the distribution of Reynolds number, $N_{R\theta}$, corresponding to each of the pressure fields, is shown in Fig. 13, and in addition, the tabulated values are presented together with the heat transfer results in Table II.

*Although this was the case assumed for blunt bodies it was of interest to see the results of such an analysis when applied to this type of body.

D. Transitional and turbulent heat transfer

1. The Reynolds analogy

To compute heat transfer rates in the regions of transitional and fully turbulent flow, the Reynolds analogy, corrected empirically for the effect of nonunity Prandtl number, may be written

$$g_w = \sigma^{-\frac{2}{3}}(h_{aw}-h_w)\,\rho_e u_e\,\frac{C_f}{2} \tag{36}$$

where the adiabatic wall enthalpy is defined in terms of the recovery factor

$$\frac{h_{aw}-h_e}{h_{se}-h_e} = \sigma^{\frac{1}{3}}$$

and the wall friction coefficient is evaluated from the boundary layer analysis.

Framing this result in terms of the Nusselt and Reynolds numbers previously defined, we write

$$N_{Nu} = \sigma^{-\frac{2}{3}}(h_{aw}-h_w)\,\rho_e u_e\,\frac{C_f}{2}\,\frac{C_{p_{se}} R_o}{k(h_{se}-h_w)}\,\frac{\mu_{se}}{\mu_{se}} \tag{37}$$

$$= \sigma^{\frac{1}{3}}\left(\frac{h_{aw}-h_w}{h_{se}-h_w}\right)\frac{\rho_e u_e R_o}{\mu_{se}}\,\frac{C_f}{2}$$

and finally

$$N_{Nu} = \sigma^{\frac{1}{3}}\left(\frac{h_{aw}-h_w}{h_{se}-h_w}\right)\frac{\bar{\rho}\,\bar{u}}{\varphi_{se}^{\frac{1}{2}}}\,\frac{C_f}{2}\,\tilde{N}_R \tag{38}$$

E. Heat transfer expressed in reference enthalpy form

For real gases, although properties across the boundary layer are known to vary with temperature, the simple assumption of a constant property fluid has been found to describe actual heat transfer processes with good accuracy, providing the properties are introduced at a suitable reference-enthalpy state. For this reason then, in reducing the experimental data to nondimensional form, local Nusselt and Reynolds numbers were defined as

$$N'_{Nu} = \frac{g_w C'_p S}{k'(h_{aw}-h_w)} \tag{39}$$

and

$$N'_R = \frac{\rho' u_e S}{\mu'} \quad , \tag{40}$$

where (for example, see reference 5), the primed quantities are evaluated at the state corresponding to the reference enthalpy:

$$h' = 0.5h_w + 0.22\sigma^{\frac{1}{3}} h_{se} + h_e(0.50-0.22\sigma^{\frac{1}{3}}) \tag{41}$$

1. Conversion of the analytical results

In order to compare the analytically predicted heat transfer results to the results of the experiment, it was necessary to convert the predicted results to the reference-enthalpy form defined above. For this purpose, the Nusselt number, N'_{Nu} was rewritten as

$$N'_{Nu} = \frac{q_w C_{p_{se}} R_o}{k_{se}(h_{se}-h_w)} \left[\frac{C'_p}{C_{p_{se}}} \frac{k_{se}}{k'} \frac{S}{R_o} \frac{1}{K}\right]$$

$$= N_{Nu}\left[\frac{\mu_{se}\bar{S}}{\mu' K}\right] \tag{42}$$

where

$$K = \frac{h_{aw}-h_w}{h_{se}-h_w}$$

The local values of the quantity $(\mu_{se}\bar{S}/\mu' K)$ thus provided for conversion from the Nusselt number, N_{Nu} used in the computer program, to the reference-enthalpy Nusselt number, N'_{Nu} in which the experimental results were expressed.

2. Comparison of predicted and experimental heating rates

From the analytical results obtained, the predictions of laminar, transitional, and turbulent heating rates over the cone-cylinder-flare configuration are presented in Fig. 11, in terms of the reference-enthalpy Nusselt number N'_{Nu}. The predictions are presented for the experimental pressure field computations, and from Table IV the results of the experimental investigation are shown for comparison.

From Fig. 11, it is seen that in the laminar flow regions, over the conical nose and the beginning of the cone-cylinder shoulder, the analytical predictions match the experimental values quite well. Also, in the transitional and turbulent regimes on the shoulder and over the forward part of the cylinder, the correlation is fairly good. However,

over the after portion of the cylinder and over the flare, the predicted heating rates are only qualitatively correct, and increasingly underestimate the actual turbulent heating rate.

3. The F.P.R.E. method

In the investigation of reference 5, based on the heat transfer over a spherically capped cone, the flat plate reference enthalpy (F.P.R.E.) method was found to give quite accurate predictions of fully developed heating rates. It was thus of interest to determine whether this simple method would result in a satisfactory prediction of heating rates in the turbulent regime of the present cone-cylinder-flare configuration.

On the basis of the local reference enthalpy Nusselt and Reynolds numbers used herein, the basic formula for the F.P.R.E. method is:

$$N'_{Nu} = 0.030\,\sigma^{\frac{1}{3}}(N'_R)^{\frac{4}{5}} \tag{43}$$

The results of the computation for the present problem have been added to the plot of Fig. 11, and although the heating rate is more closely predicted over the aft portion of the body, the F.P.R.E. method is seen consistently to overestimate the heating rate over the forward portion of the cylinder.

4. Transition point adjustment

From inspection of the experimental heating rate distribution (see Fig. 3a), a sharp increase is seen to occur at approximately the

station S=8.4 inches. Since this behavior is generally characteristic of transition to turbulent flow, it was suspected that the previous conclusions concerning the location of the laminar to turbulent transition point might have been in error. Accordingly, to investigate this possibility, the transition point was empirically adjusted to this location, and the complete turbulent boundary layer and heat transfer calculation was repeated, using the Bendix G-15 computer routine.* The results of this computation are added to the plot of Fig. 11, and as seen, no significant change in the heat transfer rate prediction is obtained. In fact, the resulting predictions are slightly lower. The tabulated results are presented in Table III.

F. Present analysis

It has been shown in the previous section that the modification of the method of Persh, as presented by reference 5, yielded an unsatisfactory result. This may be attributed to the fact that the method of reference 5 applies only to blunt bodies which have a low surface Mach number, as in the case of the laminar theory of Lees. In this theory a form factor of $H_c = -1$ was assumed, consistent with the cold wall assumption of Lees. One can envisage a negative displacement thickness on a blunt body; however, for the body under investigation, this is not possible, since the local surface Mach number is fairly high. Based on the above conclusions, and the fact that the F.P.R.E. method yield good results in the fully developed turbulent region on the flare, a method

*Extension of the laminar calculation to S=8.4" gave $(N_{R\theta})_{trans}=802$, for start of this calculation.

similar to method 5 was adopted for the transitional region, only in this case the F.P.R.E. method was adopted throughout the transitional and turbulent calculations. This will ensure that the value of the fully developed turbulent boundary layer will match the value as calculated by the F.P.R.E. method. Furthermore, the present method requires no integration of the momentum equation and may be calculated rapidly to yield the transitional and turbulent heat transfer on the body. In terms of the reference enthalpy method, the following procedure is followed.

The skin friction in terms of the reference enthalpy method is given as

$$\frac{C_f}{2} = \frac{0.332}{(N_R')^{\frac{1}{2}}} \quad \text{(Laminar Flow)} \tag{44}$$

$$\frac{C_f}{2} = (.0296)/(N_R')^{0.2} \quad \text{(Turbulent Flow)} \tag{45}$$

To evaluate the wall friction coefficient in the transitional and fully turbulent flow regimes, the skin friction low of reference 5 may be modified and written in the following way:

$$\frac{C_f}{2} = \frac{.0296}{N_R'^{0.2}} + \frac{B_1}{N_R'^{2}} \tag{46}$$

where n=1 for pressure gradient and n=2 for zero pressure gradient.

Eq. (46) may be written in terms of N'_{Nu}

$$N'_{Nu} = 0.030\,\sigma^{\frac{1}{3}}(N'_R)^{\frac{4}{5}} - \frac{B}{N'_R} \tag{47}$$

In this case the constant B is evaluated such that the heat transfer N'_{Nu} given by Eq. (46) is continuous at the laminar to transitional

$$B = N'_R[.03\,\sigma^{\frac{1}{3}} N'^{\frac{4}{5}}_R - N'_{Nu}] \tag{48}$$

In the case of test no. 1 transition occurs at the beginning of the cylinder.

$$(N'_R)\ \text{Transition} = 4\text{x}10^4$$

$$(N'_{Nu})\ \text{Transition} = 50$$

Therefore B may be determined for Eq. (48)

$$B = 350\text{x}10^4$$

The result of such an analysis is included in Fig. 11. It is seen that very good agreement is obtained for this method when compared to the experimental results.

SECTION V

CONCLUSION

An analytical investigation has been conducted for prediction of the boundary layer behavior and heating rates over a cone-cylinder-flare configuration at a Mach number ahead of the body equal to 8.0,

and with a free stream to model wall enthalpy ratio equal of 3.6 and 10.

Based on a comparison of the theoretical heat transfer predictions with experimental measurements, it is found that excellent results are obtained in the laminar region by using the transformation of Lees and the method of similar solutions. Even in the shoulder region joining the cone and cylinder, the predictions are quite good in spite of the presence of severe favorable pressure gradients.

In the turbulent flow region extending over the cylinder and flare, however, attempts at predicting the heat transfer rate, based on the boundary layer behavior obtained from a modification of the momentum integral method of Persh, were rather discouraging. Although the results obtained were found to be qualitatively correct, they consistently underestimated the actual heating rates; the agreement became poorest over the after portion of the cylinder and over the flare. Hence, for practical prediction of the transitional and turbulent heating rates, the modified momentum integral method did not yield satisfactory results.

A modified equation for the heat transfer coefficient in the transitional and fully turbulent region based on the F.P.R.E. method is presented. This method gave good predictions of the heat transfer over the entire range of transition and fully developed turbulent region.

From these results it is concluded that cooling the wall delayed transition. By expanding the flow rapidly between the cone and the cylinder, the transition Reynolds number is reached very

rapidly. The transitional and turbulent heat transfer in the presence of an adverse pressure gradient may be predicted with sufficient accuracy by the F.P.R.E. method.

SECTION VI

REFERENCES

1. Cohen, C. B. and Reshotko, E.: Similar Solutions for the Compressible Laminar Boundary Layer with Heat Transfer and Pressure Gradient. NACA TN 3325, February 1955.
2. Beckwith, I. E. and Cohen, N. B.: Application of Similar Solutions to Calculation of Laminar Heat Transfer on Bodies with Yaw and Large Pressure Gradient in High-Speed Flow. NASA TN D-625, January 1961.
3. Lees, L.: Laminar Heat Transfer Over Blunt-Nosed Bodies at Hypersonic Flight Speeds. Jet Propulsion, 26, 4, pp. 259-269, April 1956.
4. Persh, J.: A Procedure for Calculating the Boundary Layer Development in the Region of Transition from Laminar to Turbulent Flow. USNOL NAVORD Report 4438, March 1957.
5. Cresci, R. J., MacKenzie, D. A., and Libby, P. A.: An Investigation of Laminar, Transitional, and Turbulent Heat Transfer on a Blunt-Nosed Bodies in Hypersonic Flow. J. Aero. Sci., 27, 6, pp. 401-414, June 1960.

6. Rumsey, C. B. and Lee, D. B.: Measurements of Aerodynamic Heat Transfer on a 15° Cone-Cylinder-Flare Configuration in Free Flight at Mach Numbers up to 4.7. NASA TN D-824, May 1961.

7. Bland, W. M. Jr. and Kolenkiewicz, R.: Free Flight Pressure Measurements Over a Flare-Stabilized Rocket Model with a Modified von Karman Nose for Mach Numbers up to 4.3. NACA RM L57J24, January 1958.

8. Messing, W. E., Rabb, L., and Disher, J. H.: Preliminary Drag and Heat-Transfer Data Obtained from Air-Launched Cone-Cylinder Test Vehicle Over a Mach Number Range from 1.5 to 5.18. NACA RM E53104, November 1953.

9. Ferri, A.: Some Heat Transfer Problems in Hypersonic Flow. Polytechnic Institute of Brooklyn, PIBAL Report No. 473, WADC TN 59-308, AFOSR TN 59-806, July 1959; also paper presented at Durand Centennial Conference on Aeronautics and Astronautics, Stanford University, August 5-8, 1959.

10. Smith, A. M. O.: Rapid Laminar Boundary-Layer Calculations by Piecewise Application of Similar Solutions. J. Aero. Sci., 23, 10, pp. 901-912, October 1956.

11. Wisniewski, R. J. and Jack, J. R.: Recent Studies on the Effect of Cooling on Boundary-Layer Transition at Mach 4. J. Aero. Sci., 28, 3, pp. 250-251, March 1961.

12. Vaglio-Laurin, R.: Turbulent Heat Transfer on Blunt-Nosed Bodies in Two-Dimensional and General Three Dimensional Hypersonic Flow. Polytechnic Institute of Brooklyn, WADC TN 58-301, AD 206 050, September 1958.

13. Economos, C. and Libby, P. A.: A Note of Transitional Heat Transfer Under Hypersonic Conditions. J. Aero. Sci., 29, 1, pp. 101-102, January 1962.

TABLE I

THE ANALYTICAL FLOW FIELD

$M_\infty = 8.0$, $P_{S_\infty} = 600$ psia

$T_{S_\infty} = 1800^\circ R$, $T_w = 500^\circ R$

A. Conical Nose:

$$0 < \bar{S} \leq 4.695, \qquad \bar{P} = 0.4745 \times 10^{-2}$$

B. Cone-Cylinder Shoulder:

$\bar{S}$	$\bar{P} \times 10^2$
4.695	0.4745
4.887	0.3815
5.079	0.3045
5.271	0.2406
5.463	0.1886
5.655	0.1461
5.847	0.1121
6.039	0.0848
6.231	0.0635
6.423	0.0468
6.615	0.0340

C. Cylinder:

$$6.615 \leq \bar{S} \leq 23.99, \qquad \bar{P} = 0.0340 \times 10^{-2}$$

D. Flare:

$\bar{S}$	$\bar{P} \times 10^2$
23.99	0.0340
36.19	0.108

TABLE II

PREDICTION OF TRANSITIONAL AND TURBULENT
BOUNDARY LAYER DEVELOPMENT AND HEAT TRANSFER RATES

(Theoretical Transition Point, S=6.07") n=2

	n=1		n=2	
$\bar{S}$	$N_{R\theta}$	N_{Nu}	$N_{R\theta}$	$N_{Nu \times 10^{-2}}$
6.12	615.5	651.9	615.6	6.560
6.22	629.7	599.0	629.8	6.058
6.32	643.7	545.7	643.8	5.545
6.42	655.6	507.7	655.8	5.178
6.52	666.5	477.4	666.8	4.884
6.62	677.2	451.4	677.5	4.631
7.12	746.0	370.8	746.8	3.858
8.12	822.4	283.6	824.3	2.981
9.12	867.6	245.1	870.5	2.587
10.12	899.3	226.0	903.2	2.391
11.12	922.0	217.8	926.8	2.307
12.12	940.0	215.1	945.7	2.281
13.12	958.7	210.4	965.4	2.233
14.12	974.9	208.9	982.5	2.218
15.12	991.2	206.8	999.7	2.198
16.12	1006	206.4	1015.4	2.194
17.12	1020	206.3	1030.6	2.194
18.12	1032	208.1	1043.7	2.214
19.12	1042	212.2	1055.0	2.257
20.12	1054	215.0	1067.0	2.288
21.12	1062	221.0	1076.8	2.352
22.12	1072	226.5	1086.9	2.411
23.12	1078	235.2	1094.3	2.503
24.12	1080	249.8	1097.1	2.659
25.12	1075	268.6	1092.8	2.858
26.12	1060	294.2	1078.4	3.130
27.12	1039	323.4	1057.7	3.438
28.12	1013	355.7	1032.7	3.778
29.12	986.4	388.2	1005.9	4.120
30.12	957.0	423.6	976.9	4.490
31.12	926.2	463.2	946.4	4.902
32.12	895.2	506.5	915.7	5.351
33.12	863.6	558.3	884.4	5.885
34.12	831.6	625.0	852.6	6.571
35.12	800.6	709.7	821.6	7.439
36.12	772.3	821.0	793.3	8.577

TABLE III

PREDICTION OF TRANSITIONAL AND TURBULENT
BOUNDARY LAYER DEVELOPMENT AND HEAT TRANSFER RATES

(Adjusted Transition Point, S=8.4")

	n=2 Experimental Flow Field	
$\bar{S}$	$N_{R\theta}$	N_{Nu}
9.4	841.6	2.389
10.4	869.9	2.245
11.4	890.5	2.190
12.4	908.7	2.162
13.4	926.8	2.132
14.4	943.2	2.119
15.4	959.2	2.109
16.4	974.2	2.109
17.4	988.4	2.116
18.4	1000.3	2.146
19.4	1011.6	2.185
20.4	1022.6	2.227
21.4	1032.2	2.288
22.4	1041.7	2.355
23.4	1047.7	2.463
24.4	1049.2	2.625
25.4	1042.5	2.837
26.4	1026.9	3.105
27.4	1005.9	3.406
28.4	981.5	3.725
29.4	955.4	4.050
30.4	927.1	4.402
31.4	897.7	4.787
32.4	868.0	5.214
33.4	837.4	5.734
34.4	806.7	6.391
35.4	776.4	7.247
36.4	750.8	8.234

TABLE IV

EXPERIMENTAL MEASUREMENTS AND RESULTS

For the Test Point:

$M_\infty = 8.0$ $P_{S_\infty} = 590$ psia

$T_{S_\infty} = 1884^\circ R$, $T_w = 540^\circ R$

S	$\bar{P} \times 10^2$	$N'_R \times 10^{-3}$	N'_{Nu}
2.615	0.4471	146.6	227.5
3.615	0.4643	209.9	260.5
4.115	0.4541	243.7	-
5.115	0.3075	205.5	309.0
5.615	0.1754	136.0	197.5
6.115	0.0688	62.5	96.5
7.365	0.0344	33.6	54.6
8.865	0.0193	41.8	46.2
10.865	0.0206	51.0	62.9
12.865	0.0241	72.0	103.5
14.865	0.0392	67.6	119.0
16.865	0.0268	78.2	155.0
18.865	0.0227	88.0	191.0
19.865	0.0172	94.0	230.0
24.365	0.0235	102.4	173.2
25.015	0.0265	117.8	361.0
26.615	0.0330	145.3	457.0
27.365	0.0357	189.0	545.0
28.115	0.0380	208.2	640.0
28.865	0.0410	221.1	742.0
30.365	0.0460	263.9	894.0
31.865	0.0520	433.0	1115.0
33.365	0.0610	480.4	1334.0
34.115	0.0670	658.9	1417.0
34.865	0.0760	744.2	-

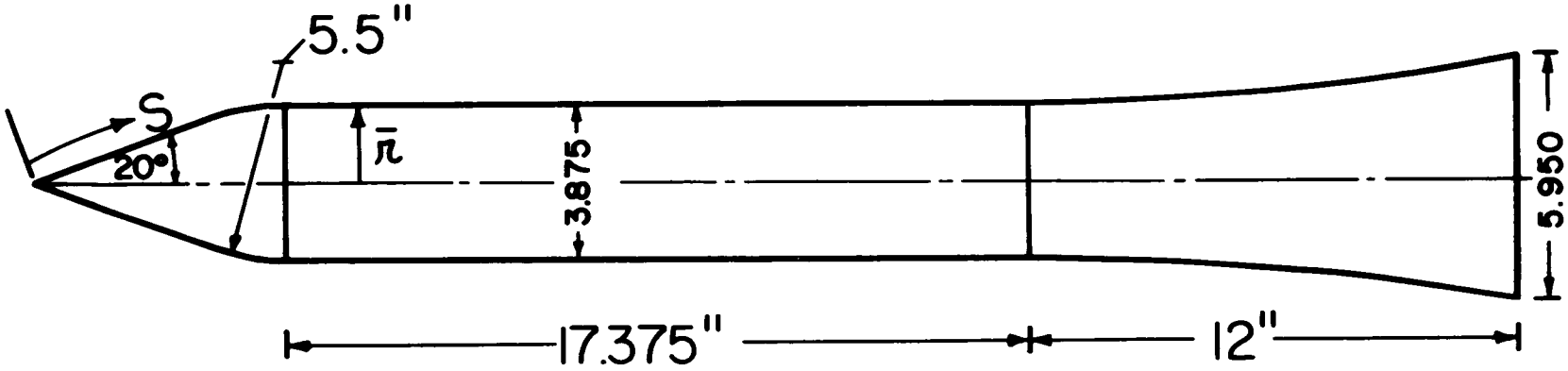

FIG. 1a. The Cone-Cylinder-Flare Configuration, Overall Model

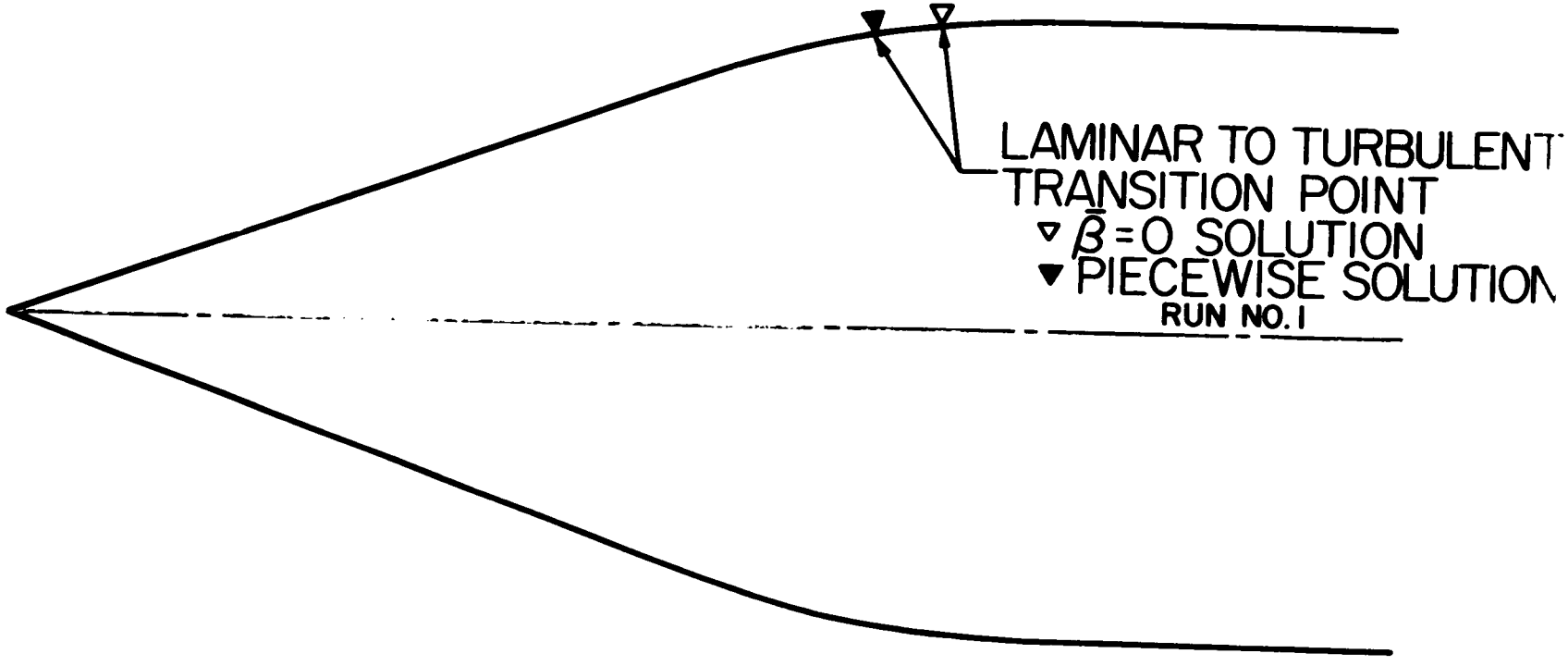

FIG. 1b. The Cone-Cylinder-Flare Configuration, Conical Nose Portion and Shoulder Region

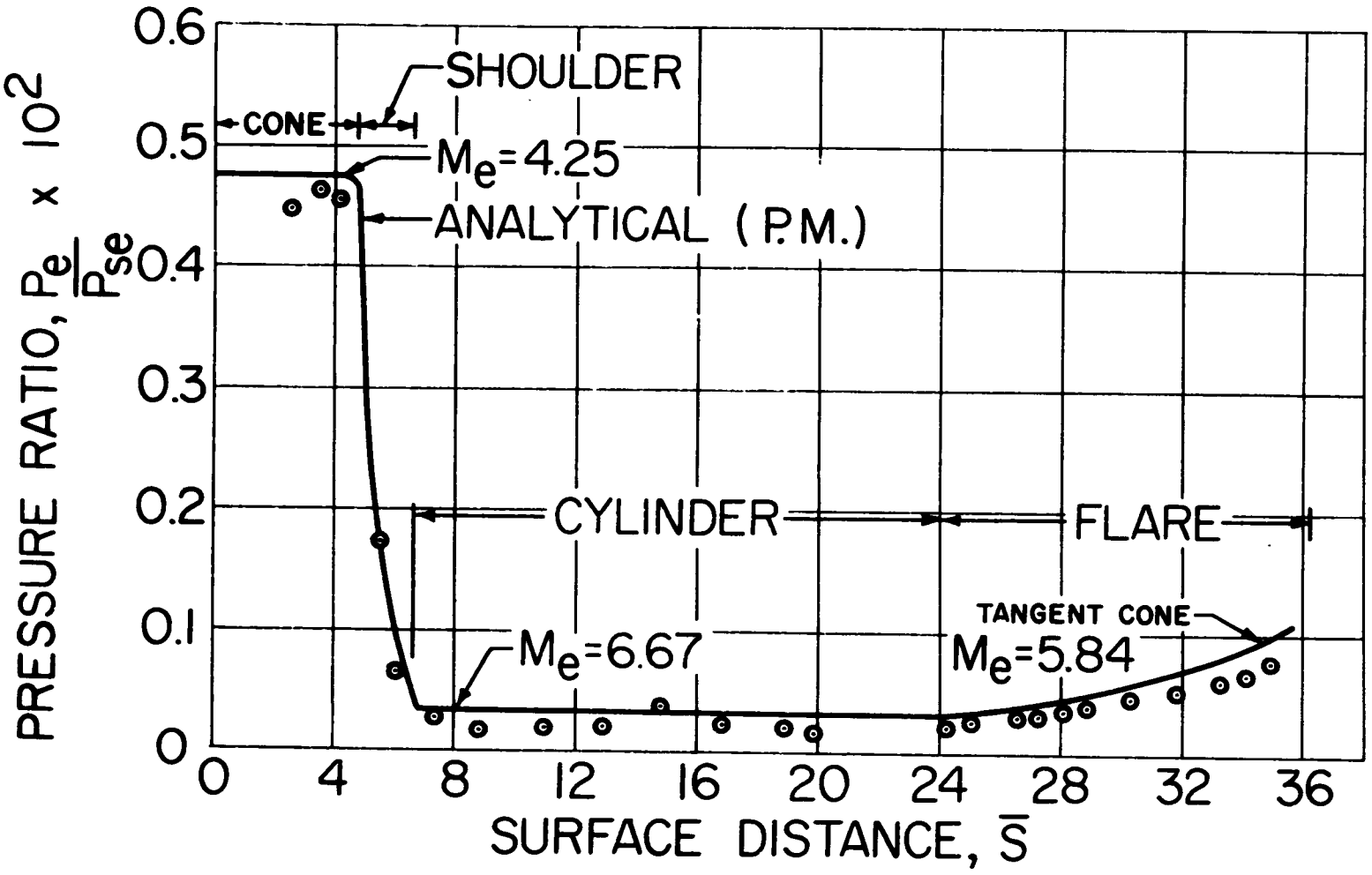

FIG. 2. Analytical and Experimental Pressure Distributions

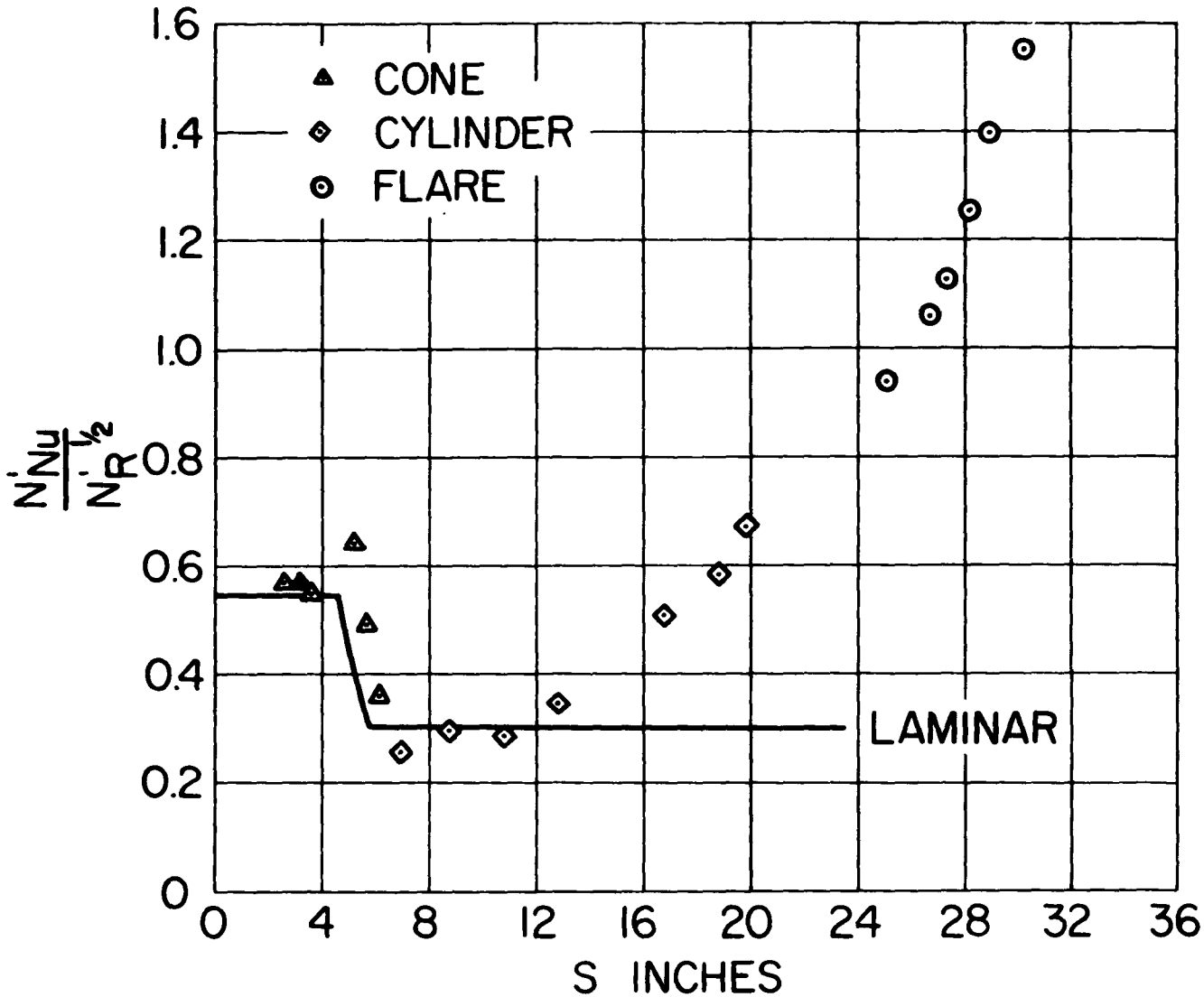

FIG. 3a. Heat Transfer Distribution Over Body in Terms of $N'_{Nu}/N'^{\frac{1}{2}}_R$ versus S(inches). Test 1.

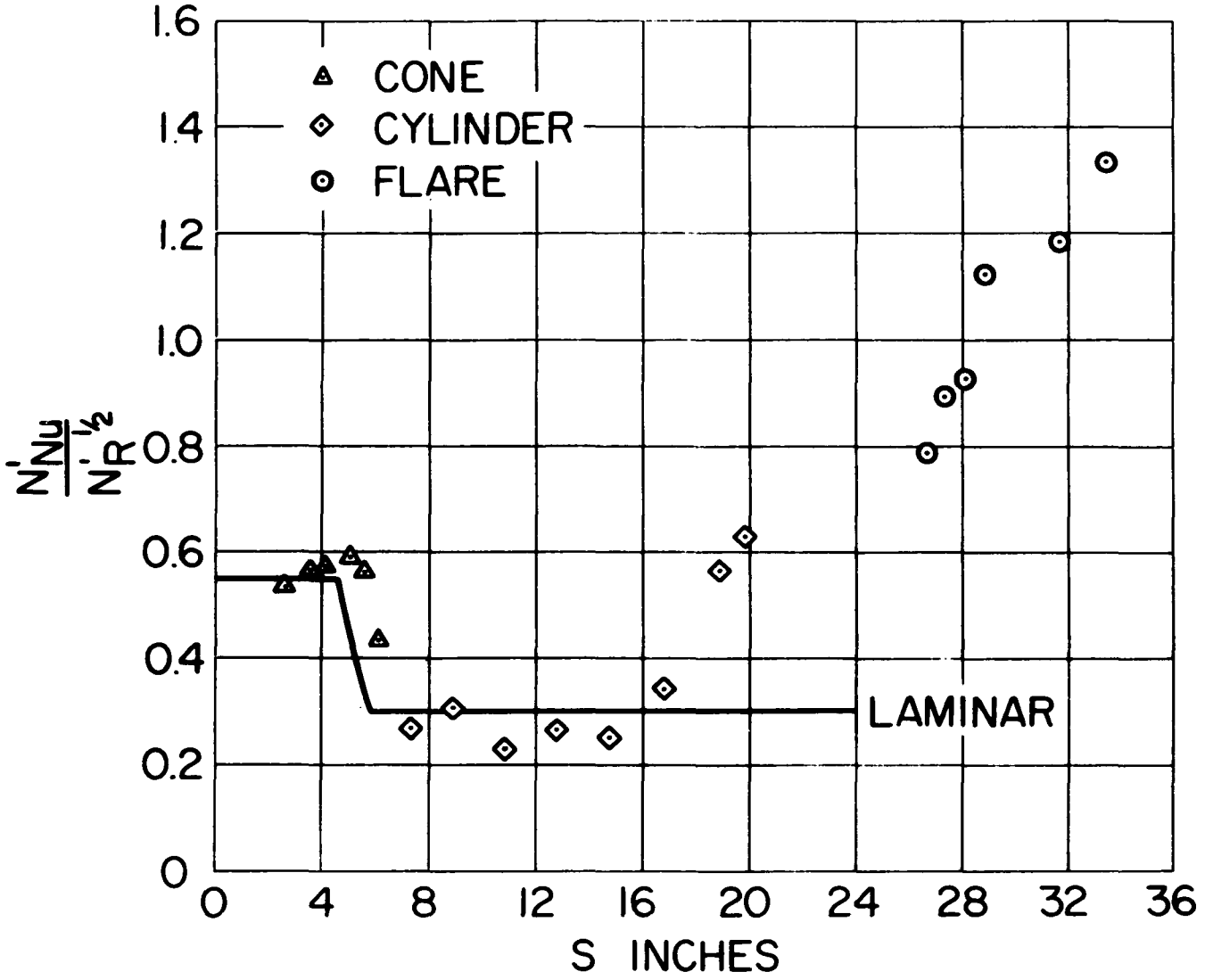

FIG. 3b. Heat Transfer Distribution Over Body in Terms of $N'_{Nu}/N'^{\frac{1}{2}}_{R}$ versus S(inches). Test 2.

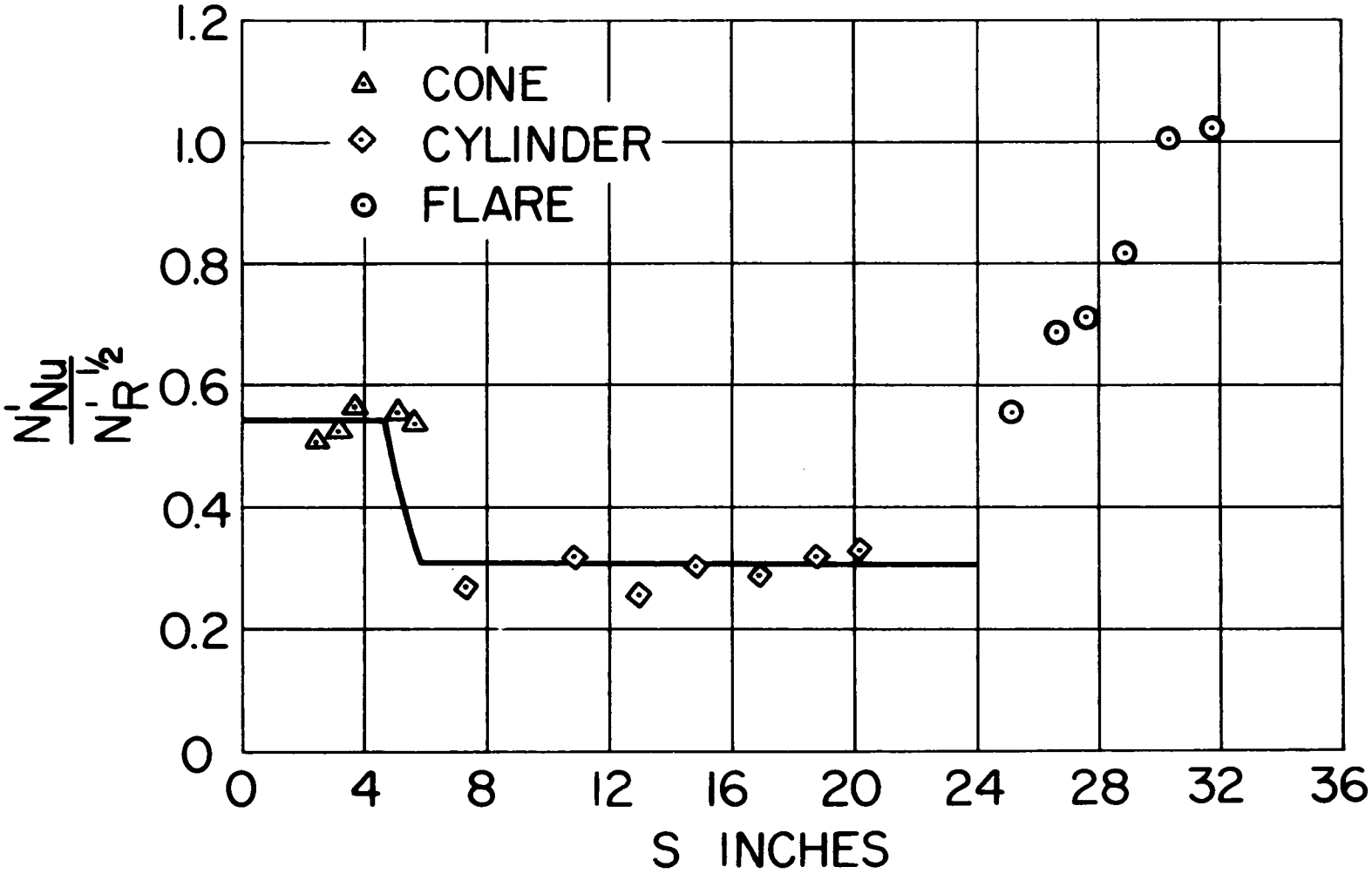

FIG. 4. Heat Transfer Distribution Over Body in Terms of $N'_{Nu}/N'^{\frac{1}{2}}_{R}$ versus S (inches), Test 3

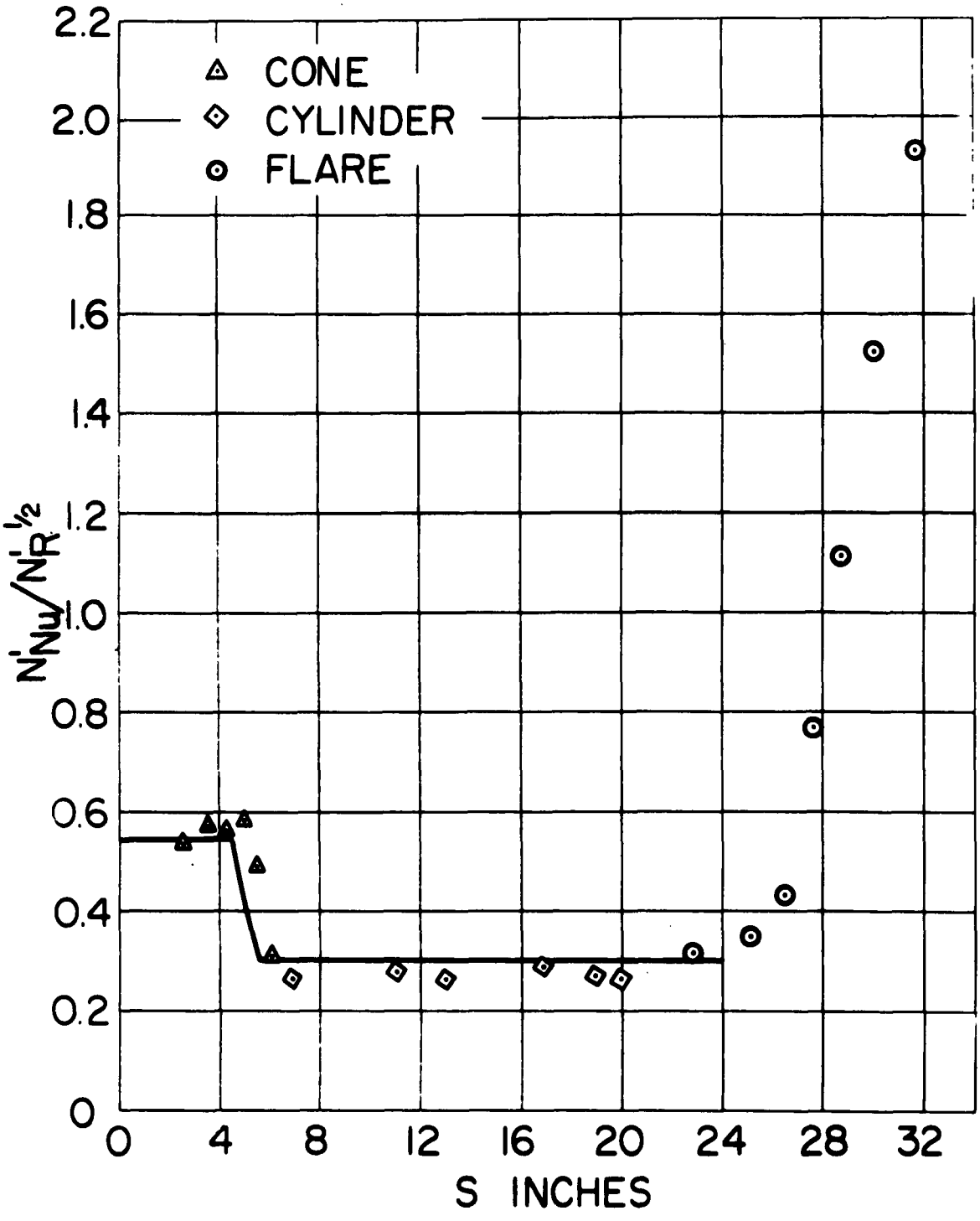

FIG 5. Heat Transfer Distribution Over Body in Terms of $N'_{Nu}/N'^{\frac{1}{2}}_{R}$ versus S(inches). Test 4.

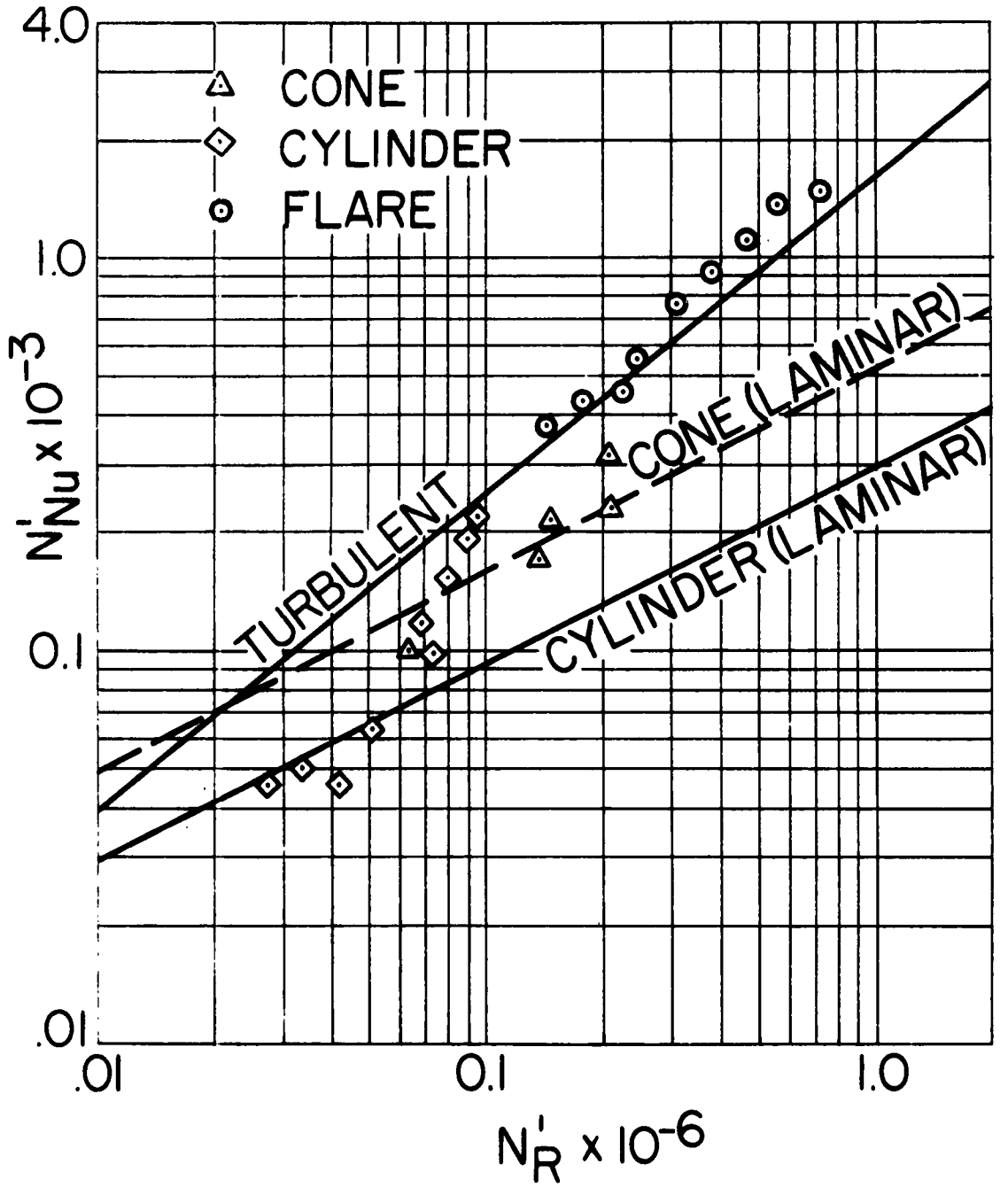

FIG. 6. Heat Transfer Results Over Body in Terms of Nu′ versus N'_R, Test 1

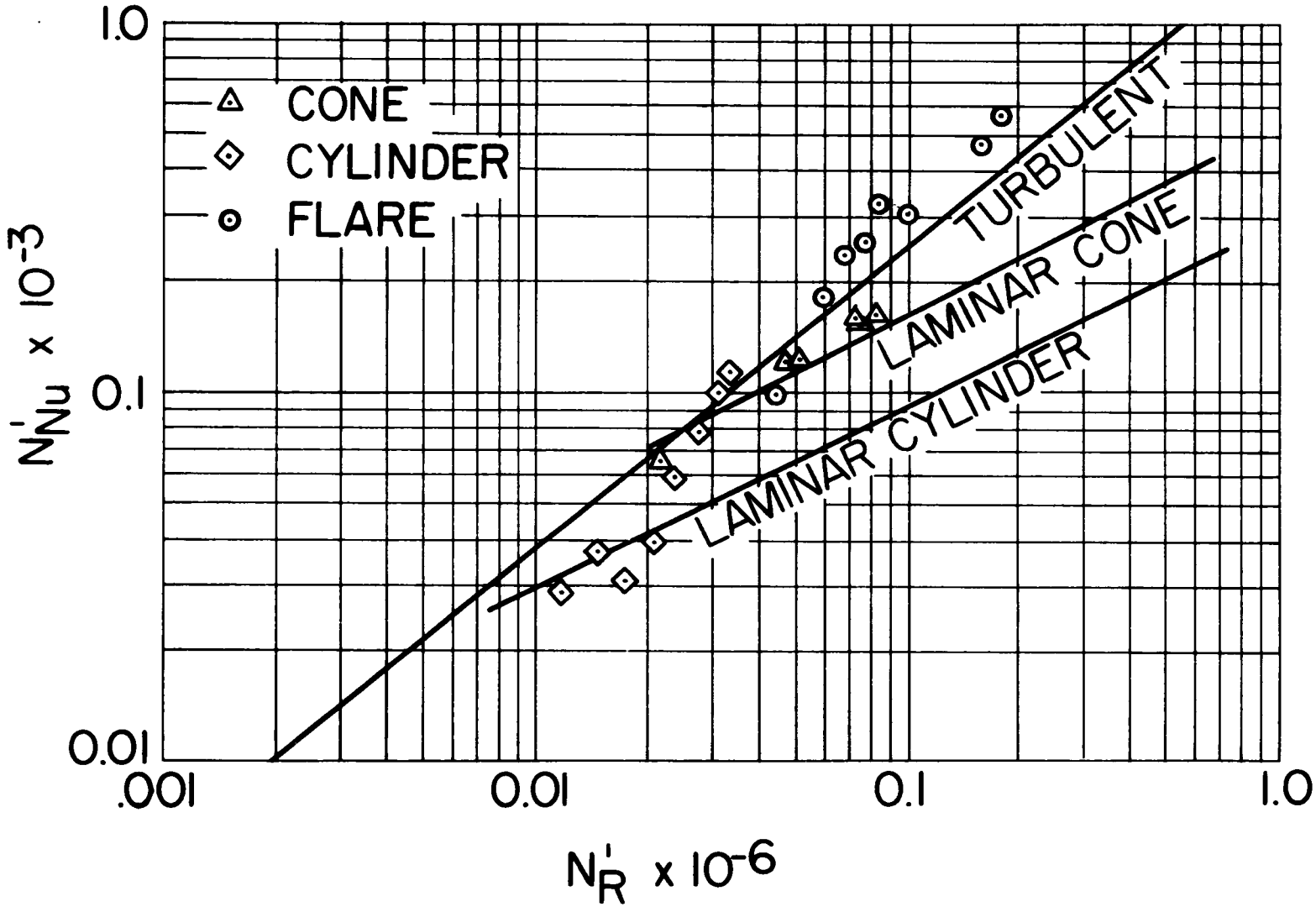

FIG. 7. Heat Transfer Results Over Body in Terms of Nu′ versus N'_R, Test 2

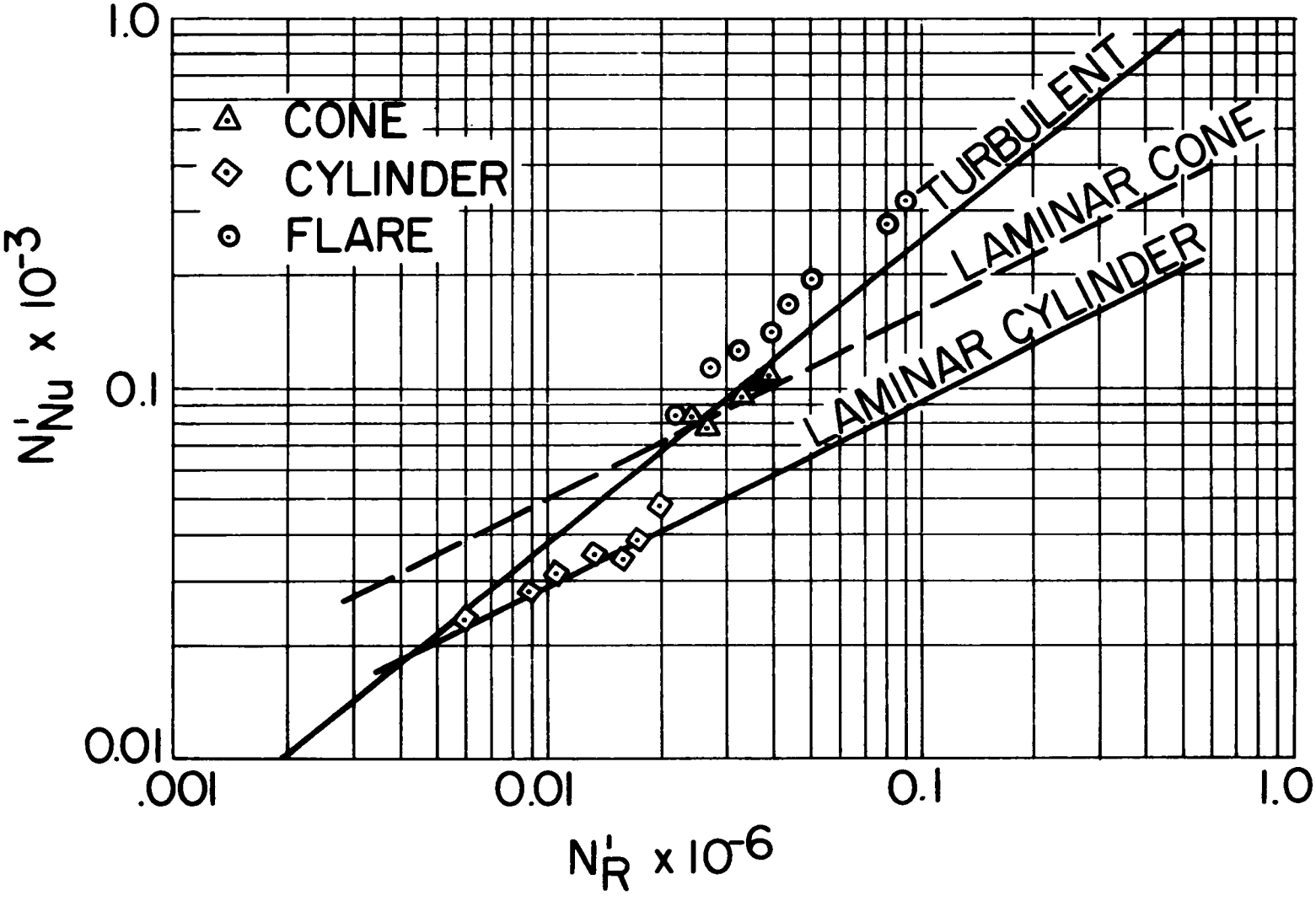

FIG. 8. Heat Transfer Results Over Body in Terms of Nu′ versus N'_R, Test 3

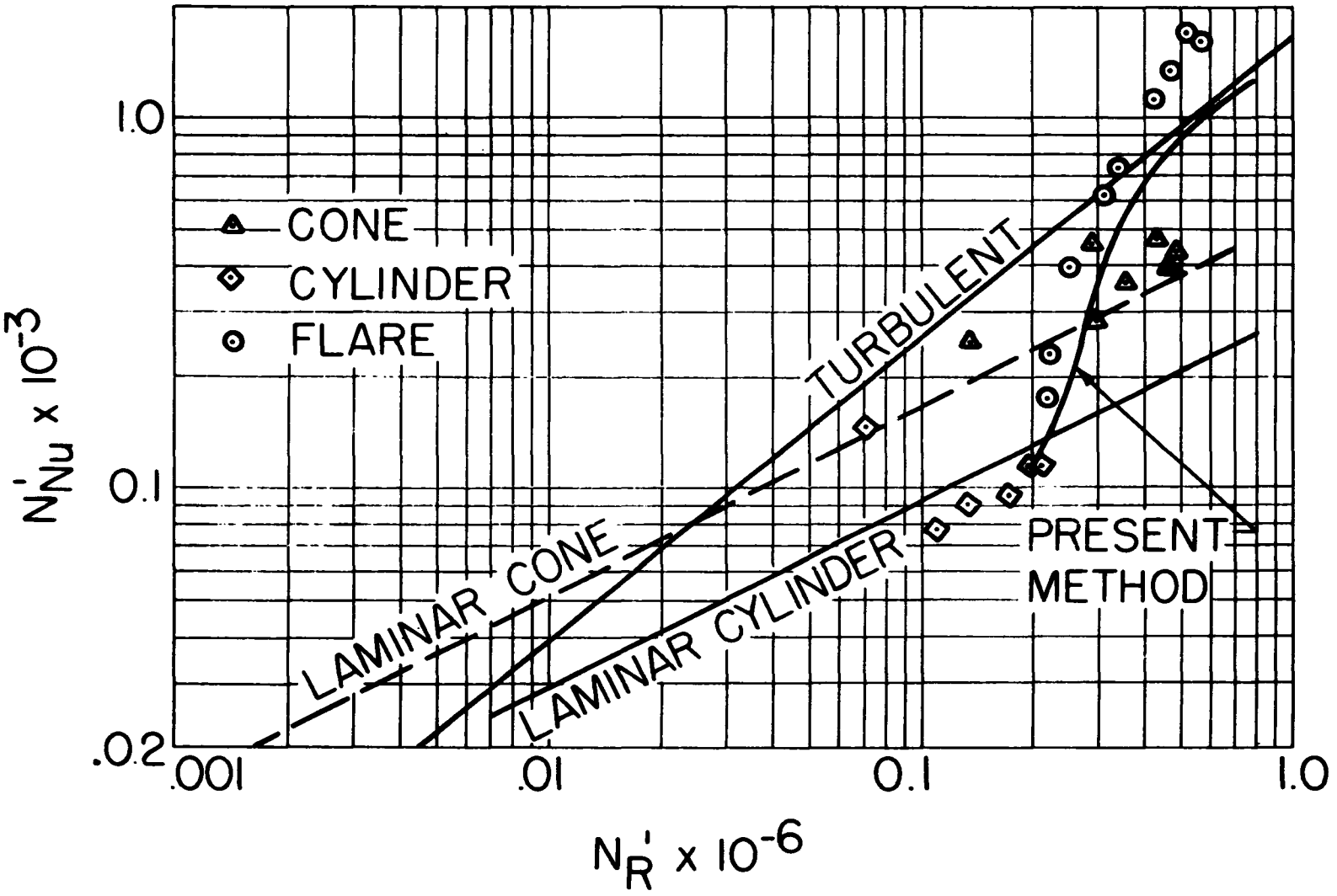

FIG. 9. Heat Transfer Results Over Body in Terms of Nu′ versus N'_R, Test 4

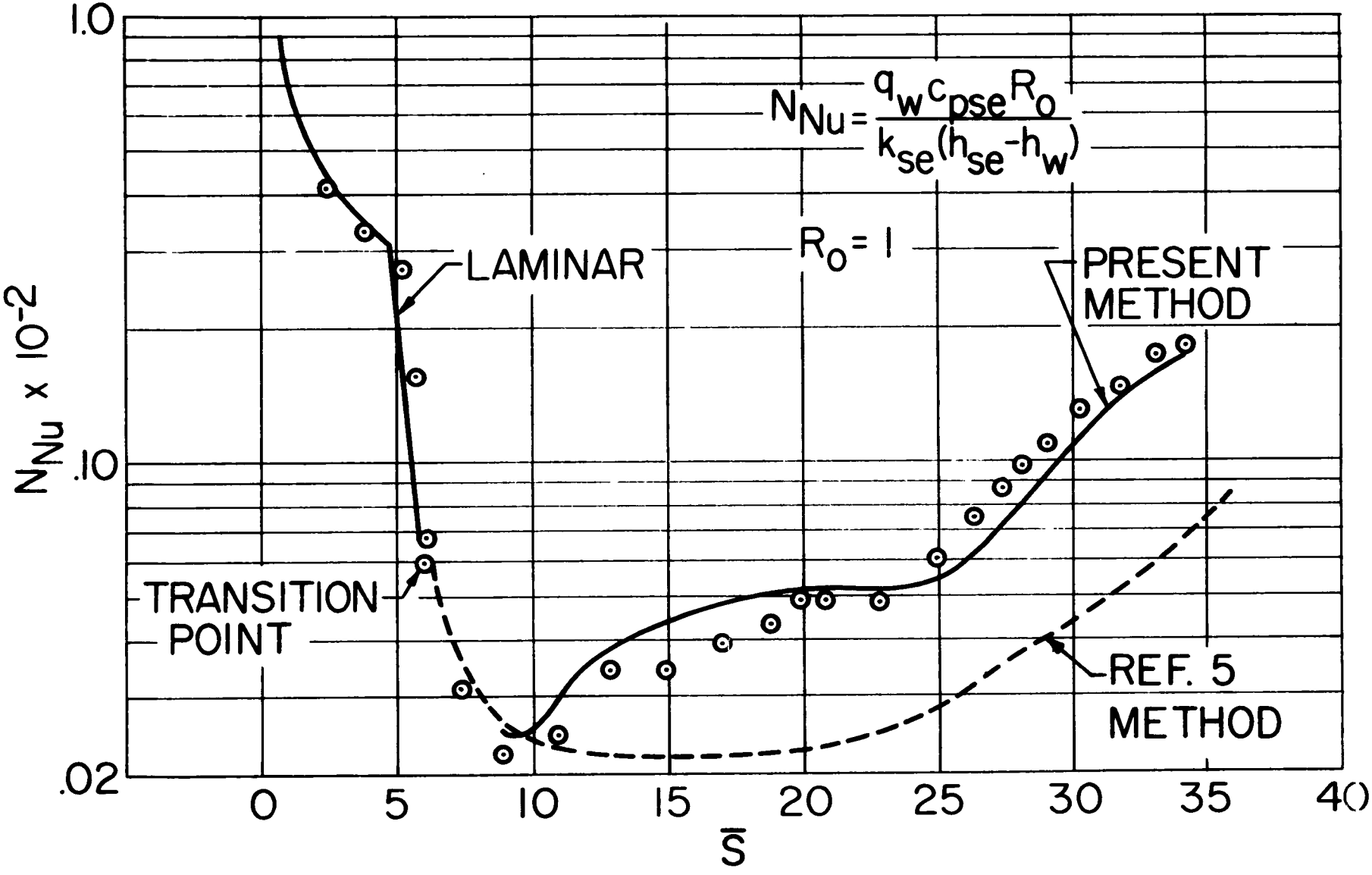

FIG. 10. Predicted Heating Rates in Terms of the Nusselt Number N_{Nu}

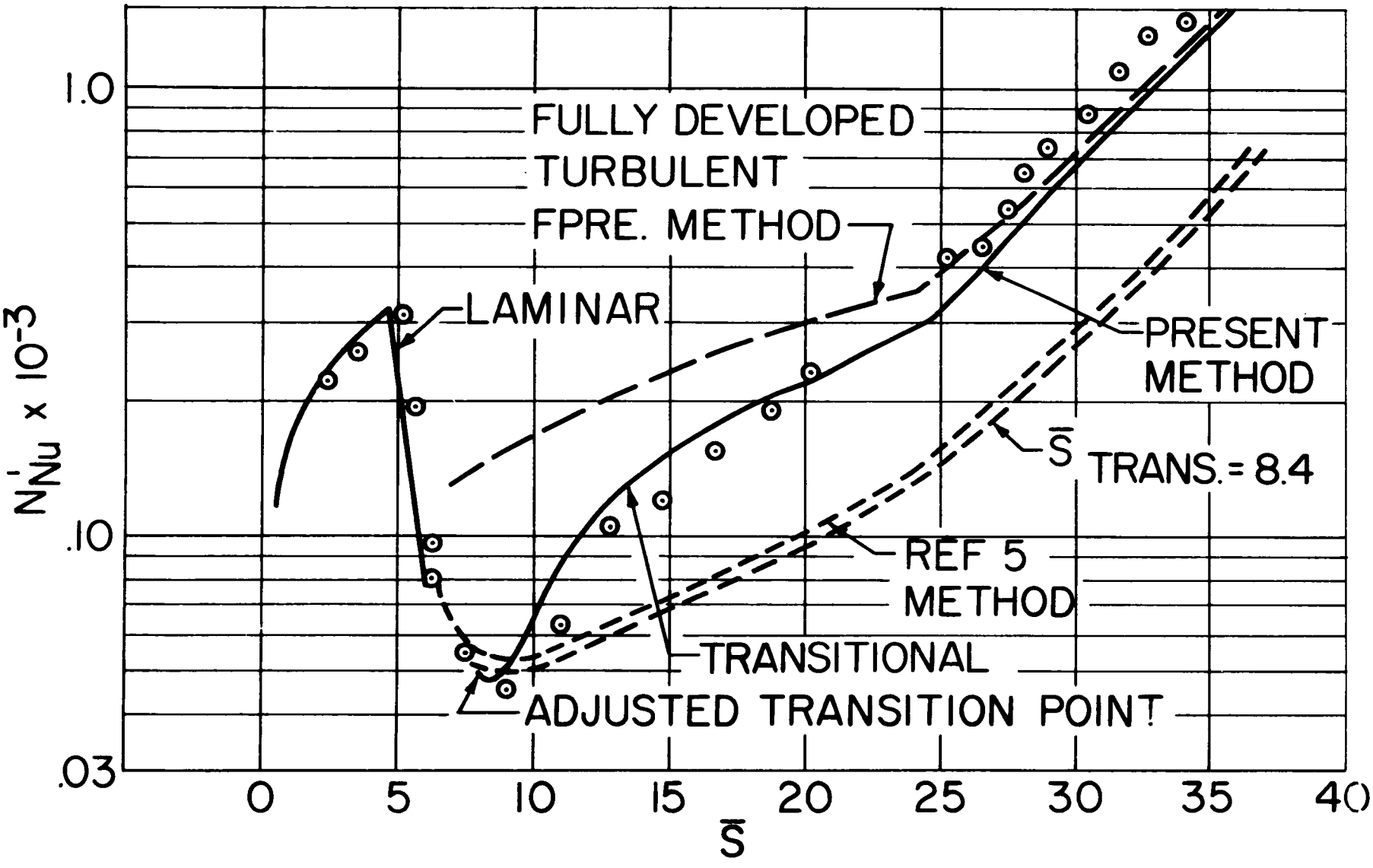

FIG. 11. Heating Rates in Terms of the Reference Enthalpy Nusselt Number N'_{Nu}

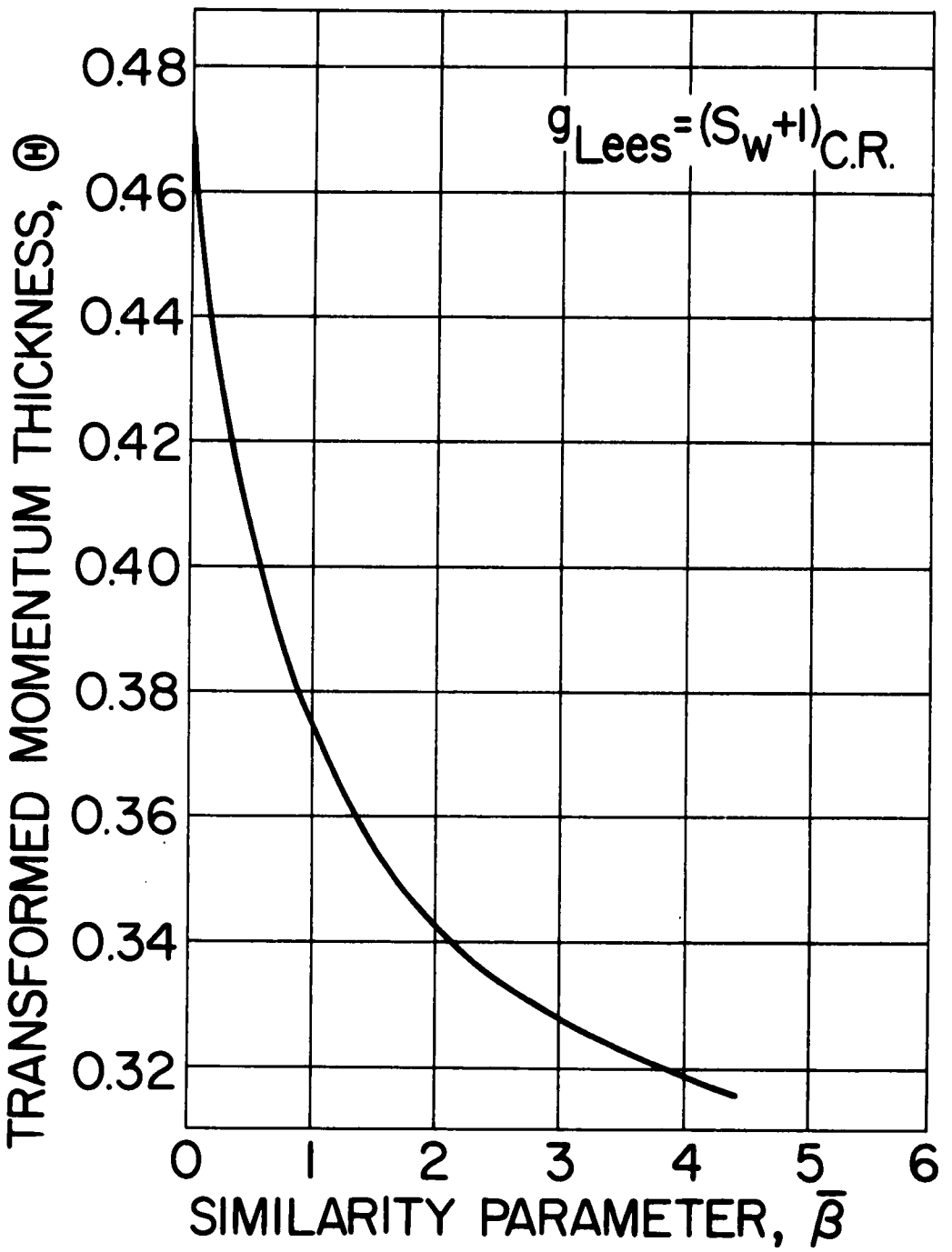

FIG. 12. The Transformed Momentum Thickness at an Enthalpy Ratio $g_w=0.2772$

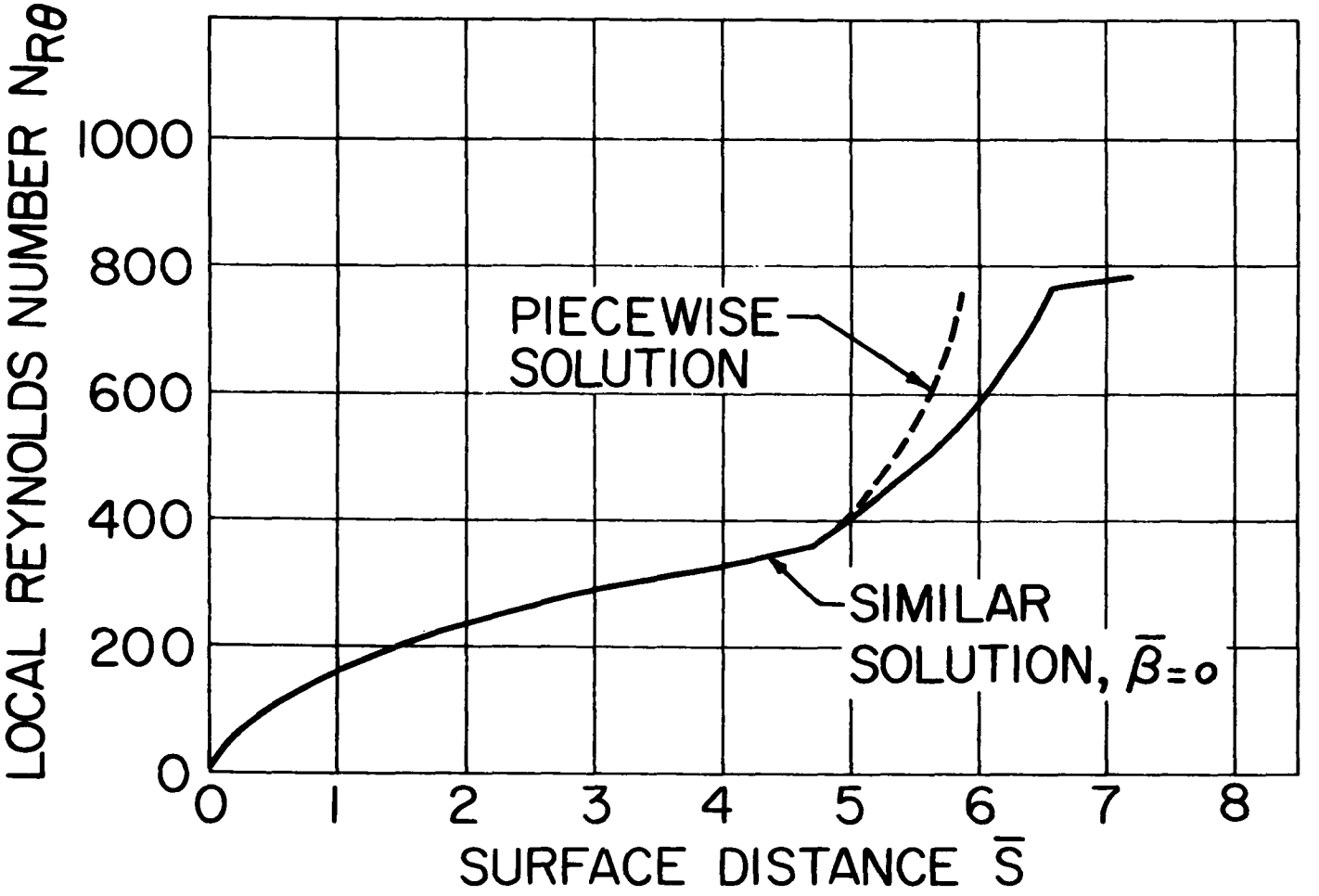

FIG. 13a. Distribution of the Reynolds Number $N_{R\theta}$ in the Laminar Region

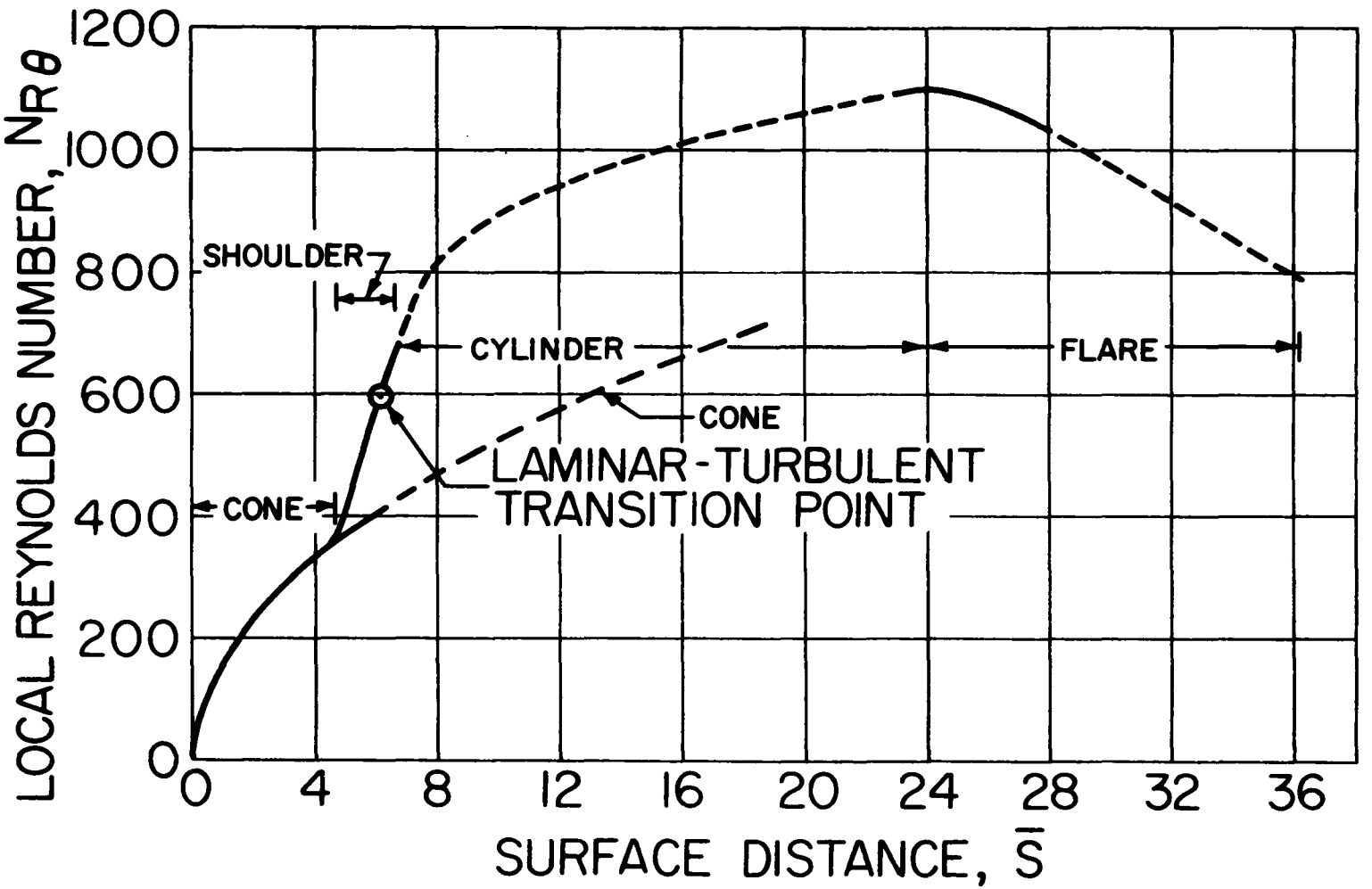

FIG. 13b. The Overall Distribution of the Reynolds Number $N_{R\theta}$

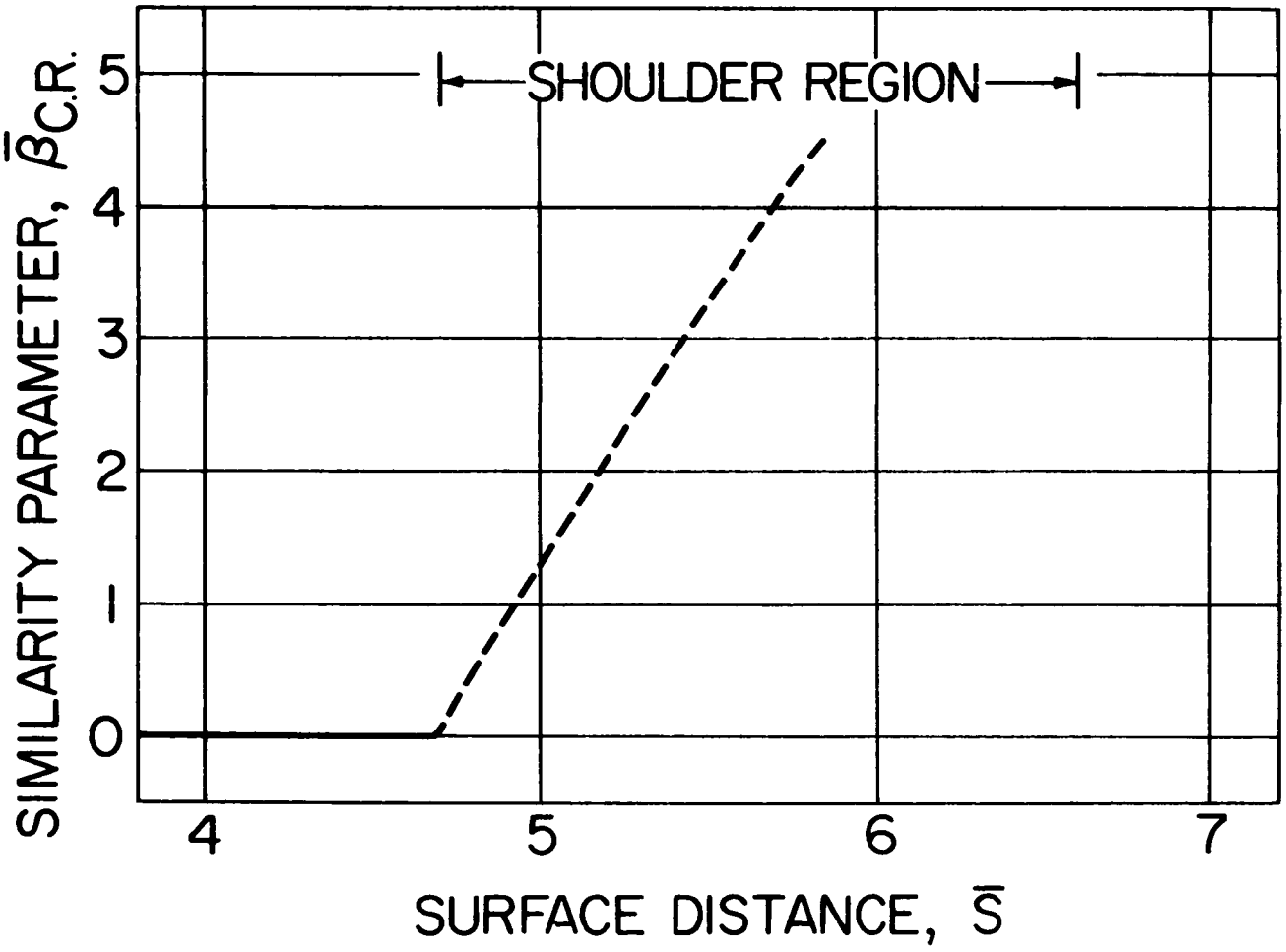

FIG. 14. Piecewise Distribution of $\bar{\beta}$ Over the Cone-Cylinder Shoulder

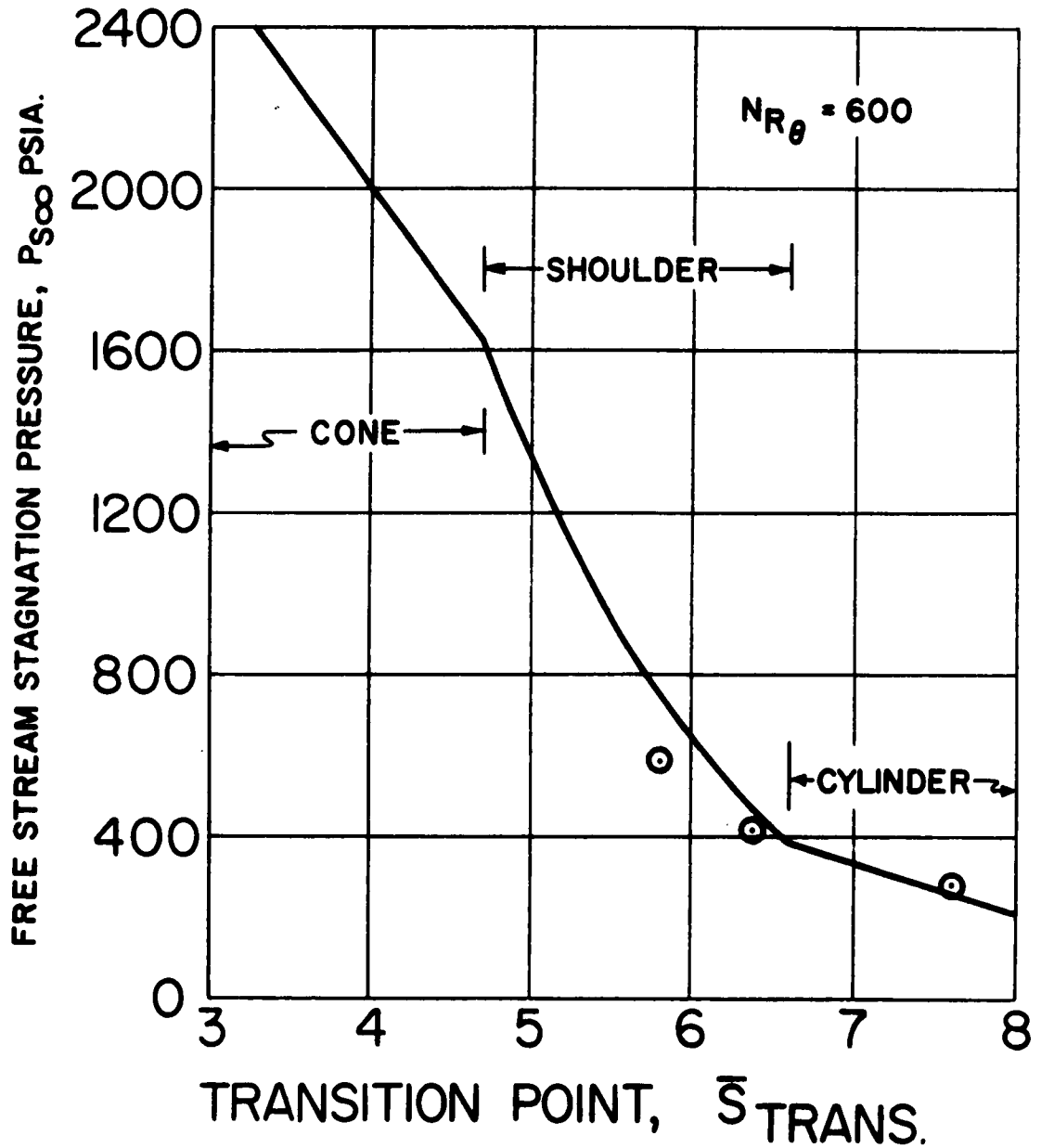

FIG. 15. The Effect of Stagnation Pressure on the Laminar to Turbulent Transition Point

Bibliographical Control Sheet

1. Originating agency and/or monitoring agency:
   O. A.: Polytechnic Institute of Brooklyn, Brooklyn, New York
   M.A.: Mechanics Division, Air Force Office of Scientific Research
2. Originating agency and/or monitoring agency report number:
   O. A.: PIBAL Report No. 737
   M.A.: AFOSR 2359
3. Title and classification of title: LAMINAR, TRANSITIONAL, AND TURBULENT HEAT TRANSFER TO A CONE-CYLINDER-FLARE BODY AT MACH 8.0 (UNCLASSIFIED)
4. Personal authors: Victor Zakkay and Clifton J. Callahan
5. Date of report: February 1962
6. Pages: 53
7. Illustrative material: 18 figures
8. Prepared for Contract No.: AF 49(638)-445
9. Prepared for Project Code and/or No.: 9781
10. Security classification: UNCLASSIFIED
11. Distribution limitations: In accordance with the approved distribution list for unclassified reports.
12. Summary. An experimental investigation of the laminar, transitional, and turbulent heat transfer rates over a conical cylindrical flared body is presented. Regions of favorable, zero, and adverse pressure gradient on the body are investigated. The experimental results are compared with the theories available in the literature.

The model chosen for this investigation is a cone-cylinder-flare configuration consisting of a 20° semi-vertex conical nose portion smoothly blended by a shoulder radius into a long cylindrical body and terminated by a smooth large radius flare.

The model was tested at a free stream Mach number of 8 and a Reynolds number of 1.6×10^{6} to 0.3×10^{6} per inch based on free stream conditions. Various stagnation-to-wall temperature ratios were obtained by cooling the model prior to the test with liquid nitrogen. The stagnation-to-wall temperature ratios ranged from 10 to 3.3.

The theoretical predictions give good results for the heat transfer rates in the laminar region, and fair prediction in the transitional and turbulent regimes extending over the shoulder and forward portion of the cylindrical body. Over the aft portion of the cylinder and over the flare the predictions are only qualitatively correct, and underestimate the heating rate by a factor as high as 2. Conversely, the "flat plate reference enthalpy" method is found more closely to predict the heat rates over the aft portion of the body, but increasingly to overestimate the heating rates over the forward portion of the cylinder.